Fabrication of TPGS decorated Etravirine loaded lipid nanocarriers as a neoteric oral bioavailability enhancer for lymphatic targeting

Abdul Muheem
Jamia Hamdard
Mohd. Wasim
Jamia Hamdard
Eman Aldosari
King Saud University
Sanjula Baboota
Jamia Hamdard
Javed Ali (javedaali@yahoo.com)
Jamia Hamdard

Research Article

Keywords: Lipid nanocarriers, LNCs, TPGS, Etravirine, HIV, AIDS, bioavailability, Lymphatic uptake

Posted Date: September 27th, 2023

DOI: https://doi.org/10.21203/rs.3.rs-3342708/v1

Additional Declarations: No competing interests reported.

Fabrication of TPGS decorated Etravirine loaded lipid nanocarriers as a neoteric oral bioavailability enhancer for lymphatic targeting.

Abdul Muheem[a]; Mohd. Wasim[b]; Eman Aldosari[c]; Sanjula Baboota[a]; Javed Ali[d,a,*]

[a]Department of Pharmaceutics, School of Pharmaceutical Education and Research, Jamia Hamdard, New Delhi, India 110062.

[b]Department of Pharmacology, School of Pharmaceutical Education and Research, Jamia Hamdard, New Delhi, India 110062.

[c]Department of Chemistry, College of Science, King Saud University, Riyadh, Saudi Arabia.

[d]Distinguished Scientist Fellow, Department of Chemistry, College of Science, King Saud University, Riyadh, Saudi Arabia.

*Corresponding author: Prof. (Dr.) Javed Ali, Email: javedaali@yahoo.com, Contact No.: +919811312247

Graphical Abstract

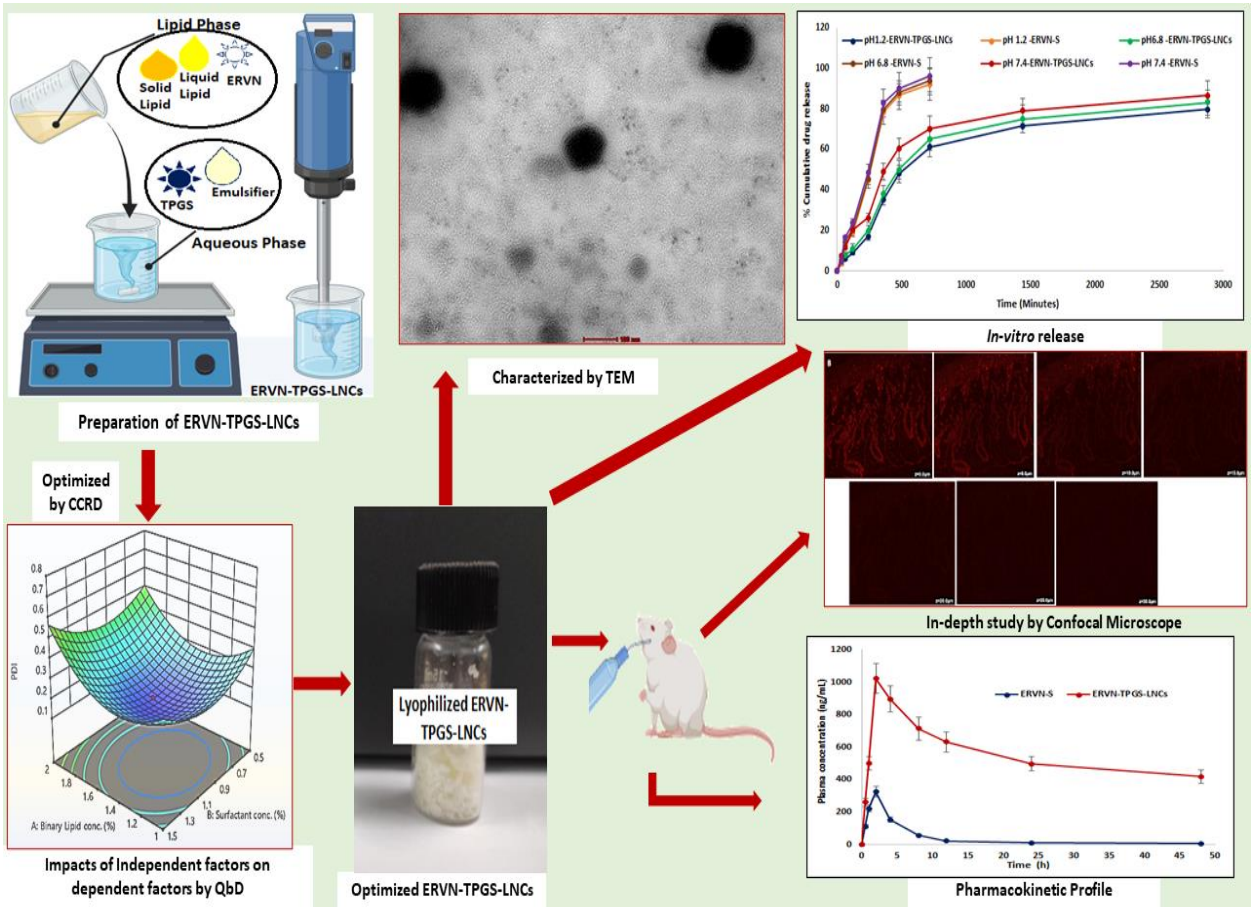

ABSTRACT

Etravirine (ERVN) is a potential NNRTI (non-nucleoside reverse transcriptase inhibitor) in treating HIV infection. It possesses extremely low oral bioavailability. The present research aims to optimize the formulation and characterization of TPGS-enriched ERVN-loaded lipid-based nanocarriers (LNCs) for HIV-infected patients. The formulation, ERVN-TPGS-LNCs, was optimized by CCRD using a modified-solvent evaporation process. Various characterization parameters of LNCs were evaluated, including globule size of 121.56 ± 2.174 nm, PDI of 0.172 ± 0.042, the zeta potential of -7.32 ± 0.021 mV, %EE of 94.42 ± 8.65% of ETR and %DL was 8.94 ± 0.759% of ERVN and spherical shape was revealed by TEM. PXRD was also performed to identify the crystallinity of the sample. *In-vitro* drug release showed % a cumulative drug release of 79.77 ± 8.35% at pH 1.2 and 83.23 ± 9.11% at pH 6.8, respectively, at the end of 48h compared to pure drug suspension (ERVN-S). Further, the intestinal permeation study and confocal microscope showed approximately ~3-fold and ~2-fold increased permeation in ERVN-TPGS-LNCs and ERVN-LNCs across the gut sac compared to ERVN-S. Hemolysis compatibility and lipolysis studies were performed to predict the *in-vivo* fate of the formulation. The pharmacokinetic study revealed a 3.13-fold increment in the relative bioavailability, which agrees with the ex-vivo studies, and lymphatic uptake was validated by using cycloheximide (CYHD) along with designed formulation, which leads to lowering AUC of ERVN-TPGS-LNCs. Thus, this study ensures that ERVN-TPGS-LNCs take lymphatic uptake to minimize the first-pass metabolism followed by improved oral bioavailability of EVN. Thus, the enhanced bioavailability of ERVN can reduce the high dose of ERVN to minimize the adverse effects related to dose-related burden.

KEYWORDS: *Lipid nanocarriers; LNCs; TPGS; Etravirine; HIV; AIDS; bioavailability; Lymphatic uptake.*

1. INTRODUCTION

Sexually transmitted diseases (STDs) and acquired immunodeficiency syndrome (AIDS) are caused by a lentivirus genus. It can be transmitted from the infected person through sexual intercourse, from the infected birth mother to their newborn, and from the infected injection [1]. The United Nations Organization (UNO) published a report where it was found that 38 million HIV-infected people were reported across the world till 2020. UNAIDS Global update-2023 revealed the declining mortality rate from AIDS and the number of HIV infections existing (38.5 million), bringing HIV infection closer to achieving sustainable development goal 3.3 towards eliminating AIDS as a public health issue by 2030 [2]. HIV usually forms sanctuaries in various body organs, including the brain, spleen, liver, kidney, lung, and lymph nodes, that infect immune cells to cause weak immunity [3]. Conversely, cellular systems such as macrophages [4] and CD4+ T cells [5] have also been reported as viral reservoirs. These sanctuaries are associated with immunity reduction. For entering into the immune cells of the human, some glycoproteins and receptors such as Glycoproteins (gp120), CXCR-4 (C-X-C chemokine receptor type 4), and CCR-5 (C-C chemokine receptor type 5) are present to the surface of viruses plays a vital role in the entry of HIV. After entering the cells, it releases the RNA of HIV into the cells and prepares the copies of the single-strand RNA, which is copied into complementary DNA (cDNA) by reverse transcriptase. The cDNAs transfer to the cell nucleus and viral proteins. It replicates over time, causing a decrease in the CD4+ T cell count. It also damages lymphoid tissues and lymph nodes to dysregulate immune function [6].

A significant challenge associated with successful anti-retroviral drugs (ARDs) delivery to viral reservoirs is due to the impermeability of drugs across the biological barriers, extensive first-pass metabolism, efflux by P-gp transporters, and gastro-intestinal degradation [7]. In addition, the

complicated dosage regimen and long-term anti-retroviral therapy (ART) cause a lack of patient compliance with medicines. Due to the presence of potential ARDs, a 39% drop has been reported in the total HIV-related death toll. Although many anti-retroviral drugs have been developed to treat viral infections, eradicating HIV remains challenging. Despite the availability of highly active antiretroviral therapy (HAART), only partial immune system improvement was reported with HAART [8]. Thus, increasing the dose of ARDs would be the only practical solution which causes higher dose-induced adverse effects to have been reported as a concern for the treatment of HIV infection [3]. The situation is more complicated for BCS II and IV drugs, as they undergo extensive hepatic metabolism and efflux by the P-gp pump, which can cause low oral bioavailability and poor drug biodistribution throughout the organs [9].

Among all the anti-retroviral drugs, Etravirine, BCS Class IV, is a second-generation potent non-nucleoside reverse transcriptase inhibitor (NNRTI) that is usually prescribed in combination with other anti-retroviral drugs to adult subjects and pediatric patients. It is available in the market as Intelence (TMC-125), which has poor water solubility and intermediate or low permeability. Its water solubility is 0.07 mg/mL, it has a high affinity for plasma proteins (99%) and an octanol-water partition coefficient (log P) greater than 5 [10]. Since the last decade, several novel formulation approaches have been explored to address the physiochemical challenges of ERVN. Due to the low solubility and dissolution rate of ERVN, this often restricts bioavailability [11]. On the other hand, CYP2C19, CYP2C19, and CYP3A4 isoenzymes of the cytochrome P450 family metabolize ERVN. The primary metabolites of ERVN (>90%) are less active against reverse transcriptase than unmetabolized ETR. Mass balance studies showed that 93.7% of the oral dose was recovered in stool and 1.2% in urine; therefore, it is a high need to develop a formulation which can bypass the hepatic metabolism [10].

To overcome ERVN-associated limitations, various bio-enabling formulation approaches have been developed to enhance oral bioavailability, e.g., complex with cyclodextrins, and amorphous dispersions [12]. However, these conventional approaches could not solve the issue related to the low solubility of the drug, leading to low bioavailability and inactive metabolite of ERVN in the system. Therefore, nanotechnology has the potential to overcome the obstacles associated with conventional formulations due to their broad characteristics, such as surface charge and particle size, which can enhance bioavailability and maintain a sustained pharmacokinetic profile [13]. Based on the size, shape, and surface properties, nanoparticles [12], conjugates [14], nanocrystals [15], liposomes, microemulsions, nanoemulsions [16], Ethosomes, self-emulsifying delivery systems [13], and cell-based nano drug delivery [17] have proven potential to improve the bioavailability of the anti-retroviral molecules. However, these drug delivery systems have several challenges, such as stability of the nanoformulation, pilot scale-up production, and complete eradication of HIV from viral reservoirs.

To enhance the delivery of ERVN to viral reservoir sites can be achieved by fabricating advanced forms of lipidic nanocarriers systems (LNCs) because solid lipid nanoparticles (SLNs) have relatively less encapsulation and drug leakage during storage. In LNCs, the drug is encapsulated in an unstructured lipid matrix of SLs and LLs to improve the bioavailability of ERVN [18]. The oral route is the simplest and safest route due to the ease of dose administration and preferable patient compliance. In the oral route, the pancreatic enzymes digest the lipid nanocarriers to mono-glycerides and fatty acids, which convert into micelles by getting entrapped by bile salts and, when reaching the enterocytes, get transform into triglycerides. Furthermore, LNCs can avoid hepatic metabolism by forming a chylomicron and then adapting lymphatic uptake [19]. The size of LNCs is generally in the range of 10 to 1000 nm, whereas particle size (less than 200 nm) for lymphatic

targeting is suitable as it assists in the easy uptake of LNCs and sustained release of ERVN. Furthermore, LNCs offer a large surface of globules for better absorption, enhancing the distribution of the drug in the brain through the oral route [20], as shown in Fig 1.

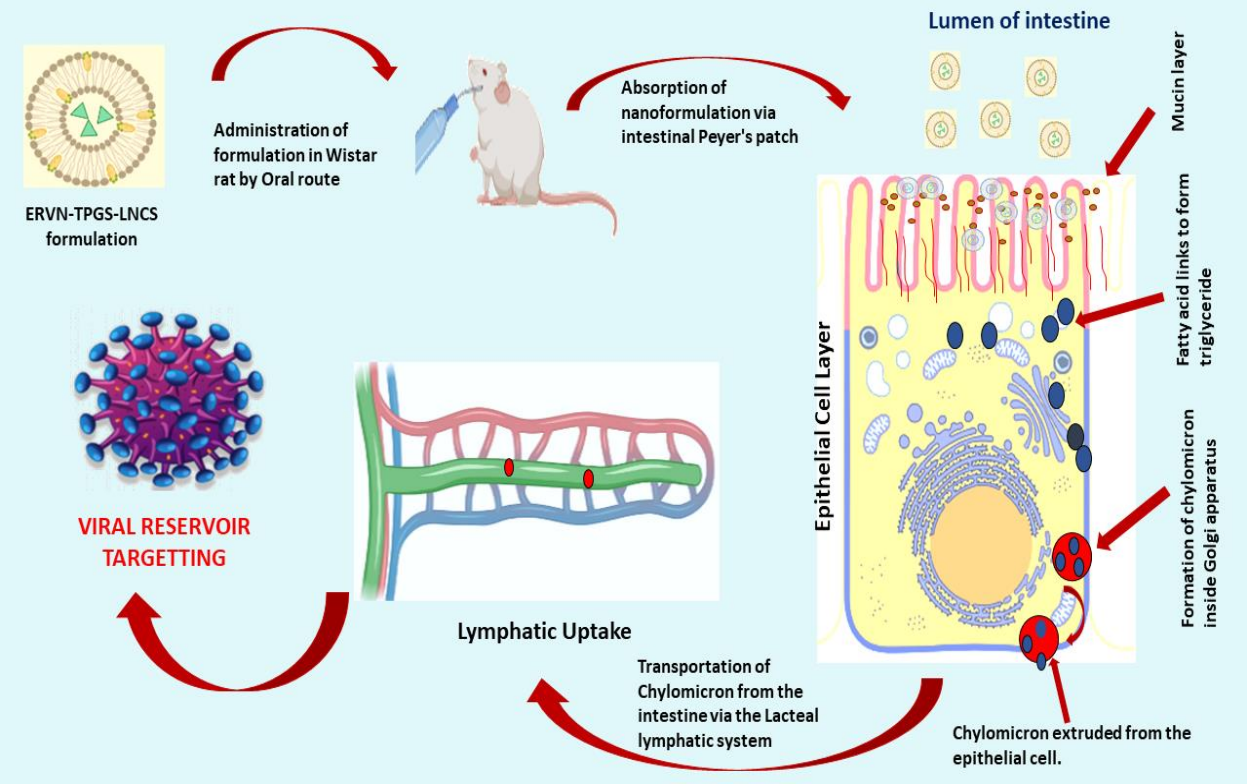

Fig 1. A schematic mechanism of ERVN-TPGS-LNCs through the lymphatic system.

This research aims to design ERVN-loaded lipid nanocarriers with TPGS via the oral route of administration and combine the results obtained from in vitro tools and a pharmacokinetic study to understand the treatment regime better. This permeation study and the in-vivo behavior of the ERVN- TPGS-loaded nanoformulation through the oral route of administration were performed to prove the anticipated hypothesis. The optimized ERVN-TPGS-LNCs were evaluated for dispersity index, globule size, zeta potential, surface morphology, in-vitro release studies, intestinal drug permeation, permeation confocal study, and pharmacokinetic studies to confirm the improvement

of oral bioavailability of ERVN leads to reducing the DRVE dose and their related adverse reactions.

2. MATERIALS AND METHODS

2.1.Materials

Etravirine was gifted by Hetero Pharmaceutical, Hyderabad, India. Vitamin E TPGS was purchased from Sigma Aldrich, India. BASF provided Labrafil M-2125 CS, Peceol, Labrafil M-1944CS, Maisine-300, Castrol oil, Plurol Oleique, Canola oil, Sesame oil, Labrasol, Capmul PG-12, Miglycol-829, Lauroglycol FCC, Captex-350, Miglycol-840, Captex-300, Neobee M-20, Labrafac WL-1349, Oleic acid, Lauroglycol-90, Capmul MCM-28, Caprol PGE-860, Precirol ATO 5, Compritol 888 ATO, Gelucire 44/14, Gelot 64, Stearic acid, Glyceryl monostearate, Apifil, Gelucire 50/13, Cremophor EL, Tween 80, Cremophore RH 40, Solutol H-15, Tween 20, and Poloxamer 407, Poloxamer 188. HPLC-grade water, methanol, and acetonitrile were purchased from Sigma Aldrich, India. Deionized water was procured from Millipore Instruments, MA, USA, available in CIF, Jamia Hamdard, New Delhi.

2.2.Methods

2.2.1. HPLC conditions for the quantification of ERVN

The concentration of ERVN was estimated through a novel developed method with binary Shimadzu LC-10A VP instruments and a variable wavelength programmable VIS/UV detector. LiChrospher C-18 (250mm × 4.6mm i.d., 5µm particle) at 30 ± 2 ˚C with acetonitrile and water in the ratio of 60:40 v/v as the optimized mobile phase [10, 11]. The flow rate, injection volume, and run time were 1 mL. minute $^{-1}$, 20µL, and 20 minutes, respectively. ERVN was estimated in samples at 309 nm, wherein the ERVN was solubilized in methanol, and the retention time (Rt)

was 10 minutes. The limit of detection (LOD) and limit of quantification (LOQ) were found to be 0.324 µg. mL^{-1} and 0.991 µg. mL^{-1}.

2.2.2. Selection of lipids

Solid lipids (SLs) and oils (LLs) were identified based on the maximum drug solubility for LNCs formulation. 500mg of each solid lipid was placed in a beaker and maintained at a temperature higher than the melting point (5 ± 0.5 ˚C) of each lipid on a magnetic stirrer. Visual observation noted the absence of transparency as the drug is saturated in SLs. An endpoint for the solubilization of ERVN was the amount of drug at which the drug did not exhibit the solubilization of ERVN [19]. Similarly, the saturated solubility of the ERVN in oils was proven by adding an extra drug to 3 mL of liquid lipids in ampoules. Small amounts of the drug were added to the lipids and vortexed in a vortex mixer (Remi Equipment, India). The lipid-filled containers were tightly closed and continuously shaken for 72 h at 25 ± 1 °C on a mechanical shaker to achieve equilibrium. The drug and liquid lipid blend were centrifuged, and the supernatants were taken out and solubilized with methanol. A UV spectrophotometer (UV1601 Instrument, Shimadzu, Japan) was used to determine the drug concentration in methanol at 311nm [21, 22].

2.2.3. Binary lipid mixture (BM) selection

The stability of the solid and liquid lipids was visibly observed in order to choose the suitable binary lipid phase. The most solubilized solid and liquid lipids were blended in this process, and transparency, turbidity, uniformity, and phase separation were assessed [23].

2.2.4. Thermal examination of a binary lipid by Differential Scanning Calorimetry

The BM ratios were selected for the ERVN-TPGS loaded lipidic nanocarrier design by applying DSC examination (DSC, Perkin Elmer, United States). Different BM ratios, such as 1:0, 9:1, 8:2,

7:3, 6:4, 5:5, and 4:6 of solid and liquid lipids, were performed while several solid lipids were mixed with increasing amounts of liquid lipids. A magnetic stirrer was used to heat this mixture of solid and liquid lipids at 80 ˚C and stir it for 1 h. It was then kept for 48 h at 25◦C ± 1 °C. These ratios of binary lipids were used to determine the percentage variation in the crystalline nature. This study employed 100% selected solid lipids as a control. The crystallinity index (CI) of BM was calculated using the following formula:

$$CI = \frac{\Delta H_{BM}}{\Delta H_{SL}}$$

ΔH_{BM} and ΔH_{SL} denote the enthalpy of binary lipid mixture and solid lipid, respectively [21].

2.2.5. Surfactant selection

Different surfactants were examined for their ability to stabilize the LNCs. The most effective emulsifiers were selected depending on their ability to fabricate stable LNCs with the smallest globule size. Furthermore, passivated surface and minimize the surface energy to reduce the globule-to-globule interactions and, as a result, to have the smallest globule size. 100mg of the BM was solubilized in 3 mL of dichloromethane (DCM) before being mixed with a 5% surfactant solution. The produced mixture was kept at 45 ± 2˚C and stirred to evaporate DCM, followed by 1 mL of the mixture being diluted with 20 mL of distilled water. The % transmittance of the mixture was measured using a UV spectrophotometer at 510 nm after diluting the mixture [24].

2.2.6. Selection of Vitamin E TPGS concentration

TPGS is an amphiphilic compound, a stabilizer, and a p-glycoprotein (p-gp) efflux inhibitor. HLB of 13.2 and CMC concentration of 0.2% w/w make them soluble in an aqueous medium. It blocks the p-gp efflux pump through various mechanisms, such as ATP reduction, substrate binding site inhibition, and membrane fluidization. Furthermore, it also acts as an emulsifier, which is a critical

feature in the fabrication of nanoformulation, along with helping to overcome biological barriers and reduce the multidrug resistance of the therapeutic molecule. It was reported that TPGS has inhibitory properties at a concentration of 0.025mM. Therefore, various concentrations of TPGS were examined for their ability to stabilize the LNC formulation. Hence, the concentration of TPGS was selected with a variable range of 0.1–1% w/w, and the prepared formulations from various concentrations were kept for one month to examine the stability of the formulation by visual observation [25]. Also, the % transmittance of the resultant mixture was measured using UV spectroscopy at 510 nm after diluting the mixture.

2.2.7. Quality by design and implementation

2.2.7.1. Allocation of critical quality attributes (CQAs) and quality target product profile (QTPP)

Quality by design (QbD) based strategy was initiated by allocating the QTPP that could be achieved with respect to a patient-centric approach, including the safety and efficacy of the final formulation. It was obtained from the recommendation of experimental justification and ICH-Q8. The crucial variables, such as dose strength, dosage form, the route of administration, and pharmacokinetic profile, were majorly focused on the targeted product.

In addition, crucial CQAs were found to have a notable effect on product quality. The CQAs were observed and managed to ensure the required product quality. These characteristics were further evaluated based on previous literature and conducted experiments [26].

2.2.7.2. Risk evaluation

Risk evaluation was performed to identify critical formulation factors such as critical material attributes (CMAs) and critical process parameters (CPPs), determining the formulation

performance. The Ishikawa diagram was formed to show high-risk factors with their corresponding cause and effect to achieve the quality of the product. Furthermore, risk evaluation has employed the factors of the effective formulation [27]. Thus, the risk estimation of the proposed formulation was conducted by combining the Ishikawa diagram and risk assessment matrix.

2.2.7.3.Formulation development of LNCs

ERVN-TPGS-loaded LNCs were designed using the modified solvent emulsification method. ERVN was added to the optimized melted BM, and half the amount of aqueous emulsifying solution was added at 80 ± 6°C, followed by stirring at 600 rpm. Next, the remaining half of the aqueous surfactant solution containing TGPS was added to the mixture with constant stirring at 700 rpm for 20 minutes at 80 ± 6°C. Then, the subsequent emulsion was ultrasonicated with an ultra-probe sonicator (Hielscher Ultrasonics, Teltow, Germany) while placing it in an ice bath and cooling to room temperature [28].

2.2.7.4.Applying CCRD for the optimization of LNCs

LNCs were fabricated using response surface methodology through Design-Expert-13.0.1.0 (State-Ease Inc., United States). Response surface methodology is a mathematical tool used to understand and comprehend the effects of combining variables [29]. Among the RSM, the CCRD was used to determine the impact of various process limitations on the responses, such as globule size (nm), PDI, and % EE. In CCRD, quantitative and statistical estimates are grouped in modeling and analyzing the hitched with variable matrices. It effectively determines how dependent variables affect the operation of the independent variables.

Furthermore, there is a decrease in the experimental trials needed to recognize the statistical trend, making evaluating the variables and levels crucial for a given response easier [30]. For the

development of a robust formulation, binary mixture (% w/w), surfactant (% w/w), and probe sonication time (seconds) were selected as the independent variables, as shown in Table 1. Their responses on globule size in nm, PDI, and entrapment efficiency (%) were examined.

Depending upon the independent input factors, CCRD generated 20 randomized formulation trails, and a quadratic polynomial equation was created to describe the impacts between independent variables (A, B, and C) and the evaluated response (R), where b was the regression coefficients and b_o was the constant. The regression coefficient (b) explained the mathematical measures of the impacts of the factors that were either curvilinear or linear and their relationships that b_{12}AB, b_{13}AC, and b_{23}BC indicated as shown in the below equation. Instead of being an actual model, this equation was considered a statistical design.

$$R = b0 + b1A + b2B + b3C + b12AB + b13AC + b23BC + b22A2 + b22B2 + b33C2$$

2.3.Characterization of optimized LNCs

2.3.1. Globule size and Polydispersity index (PDI)

Globule size and PDI of the LNCs were examined using a Zetasizer equipped with Malvern software (Malvern, UK). The concept was derived from dynamic scattering, which involved determining the variation in luminous intensity emitted by LNCs repeatedly subjected to Brownian motion. To achieve uniform dispersion, the nanoformulation was diluted tenfold in Milli-Q water, and an evaluation was carried out at a scattering angle of 90 degrees at room temperature [31]. All the measurements were conducted three times (n = 3).

2.3.2. Zeta Potential

The surface charge of the optimized LNCs was evaluated using a Zeta-sizer equipped with Malvern software (Malvern, WR14 1XZ, United Kingdom). The apparatus was calibrated using a 0.9% w/v

solution of NaCl dissolved in Milli-Q water to attain a conductivity of 50 mS/cm. The LNCs were dissolved in Milli-Q water as 50µL of nanoformulation in 10 mL of Milli-Q water. The nanoformulation was diluted to estimate the zeta potential at room temperature. All the estimations were conducted thrice (n = 3) [32].

2.3.3. Entrapment efficiency (%EE) and Drug loading (%DL)

The developed drug loaded LNCs were centrifuged at 10,000 rpm for 40 minutes using a high-speed centrifugation machine. The solid content was collected after the supernatant was discarded. To completely remove unentrapped ERVN, the solid contents were rinsed thrice with a phosphate buffer solution of pH 7.4. Then, the washed solid material was dissolved in methanol and allowed to settle for ten minutes to ensure appropriate mixing and dissolution of the lipid in the solid material. Further, UV spectroscopy determined the diluted samples for drug estimation [28]. The % EE and %DL were estimated using the below formula:

$$\%EE = \frac{W_{total} - W_{free}}{W_{total}} \times 100$$

$$\%DL = \frac{W_{total} - W_{free}}{W_{lipid}} \times 100$$

Where, W_{total} = total amount of the ERVN, W_{free} = total weight of the unentrapped drug, and W_{lipid} = amount of the lipids used in the LNCs sample.

2.3.4. Lyophilization of LNC formulation

Mannitol, a cryoprotectant, was employed to lyophilize the placebo and ERVN-TPGS-loaded LNCs. Mannitol (5% w/v) was used for dispersing the LNCs formulation, and the dispersion was stored overnight at a freezing temperature (-20°C) [33]. The frozen samples were kept at -20°C for 16 hours in a lyophilizer (LABFREEZ instruments, FD-10-R, China), followed by a freeze-

dried sample. The obtained freeze-dried powder was collected to perform several characterization parameters on LNCs.

2.3.5. Surface morphology by Transmission Electron Microscope (TEM)

LNC formulation was used to prepare the sample by dilution 10-fold with Milli-Q water, and then the diluted sample was placed in a copper mesh grid coated with a carbon layer. Next, the sample was stained with 1% phosphor-tungstic acid for negative staining, and the grid mesh was placed to dry in the open air. Finally, the sample was placed in a copper grid of TEM (Fei Company, Netherlands) [24]. The sample was examined in improved magnification along with various diffraction modes that provide brightfield imaging to get the size and shape of the LNCs formulation.

2.3.6. Powdered X-Ray Diffraction (PXRD)

XRD was performed using X'Pert PRO (PANalytical, UK) to identify the crystallinity of the sample. To determine the crystallinity of the samples, different slits were set at 49 kilovolts. The scan was conducted from 5 to 80 degrees at two theta positions at 25 ± 2 °C with 65–70% humidity [34].

2.3.7. Chemical analysis of LNCs by FT-IR spectroscopy

The sample was blended with KBr in a 1:50 (w/w) proportion for structural investigation by Fourier transform infrared FT-IR by Bruker. The mixture was prepared by triturating it in a mortar and pestle to form a super fine particle, which was then pressed into pellets by hydraulic pressure [22]. The pellets were used for chemical analysis of the sample by FT-IR spectroscopy.

2.3.8. Thermal analysis of drug in LNCs by DSC

A Thermal examination was carried out using DSC to identify the encapsulation of ERVN in the optimized nanoformulation. First, 10mg of the sample was packed in an aluminum pan exposed to a DSC run over a temperature of 30-400°C. For a reference sample, an empty pan was used. Then, nitrogen purging was used while recording and analyzing the thermogram [28].

2.3.9. Drug release studies using dialysis-bag

An in-vitro drug release examination of the LNCs was conducted utilizing dialysis membranes in different buffer solutions. The dialysis bag must be activated before performing a drug release study, where glycerin must be removed from the dialysis bag by immersing it in continuous running water for three to four hours. Then 0.3% w/v sodium sulfide (Na_2S) was used to rinse the dialysis bag at 80°C temperature for 1 minute to separate sulfur contents. Further, sulfur and sodium sulfide were cleaned for two minutes in heated water (70°C). In order to acidify the dialysis bag, 0.2%v/v of sulfuric acid was used to rinse the remaining sulfuric acid with hot water [35].

ERVN release from ERVN-TPGS-loaded LNCs and its correspondence suspension (ERVN-S) were studied using an activated dialysis membrane in different buffers. Each formulation, 3mL, was placed into a dialysis membrane, which was then tied at both ends to produce a bag-like shape. The closed bag was placed in 100 mL of dissolution mediums (0.1N HCl-pH 1.2, and PBS-pH 6.8) with 1% w/v sodium lauryl sulfate (SLS) at stirring of 100 rpm and maintained the temperature of 37 ± 0.5°C on the magnetic mixer. A three mL aliquot was collected at 0.5, 1, 2, 4, 8, 12, 24, and 48 hours. The equivalent volume was replaced with the dissolution media to maintain the sink state. UV spectroscopy was used to evaluate the drug content of the sample. The drug release outline was compared with respect to the % CDR and similarity function (f_2).

Using kinetic models, the drug release study from LNC formulations was compared with the suspension of ERVN. The suitable kinetic model was chosen to depend on a regression coefficient close to 1. The "n" value exhibited in the equations of different kinetic models shows the release mechanism of ERVN (n values lie in the range of 0.43 to 0.85). Fickian diffusion occurs when n values are less than or equal to 0.43. Suppose n values are present in the 0.43 to 0.84, which follows non-fickian diffusion. Conversely, the n values lie greater than or equal to 0.85 and follow the zero-order kinetics [36]. % cumulative drug release was calculated by using the following formula.

$$\%\ Cumulative\ Drug\ release = \frac{Conc.\ (\mu g/mL) \times Volume\ of\ release\ medium\ (mL) \times Dilution\ factor}{initial\ dose\ (\mu g)} \times 100$$

2.3.10. *In-vitro* lipolysis

A lipolysis study was performed to determine the in-vivo simulation of LNCs at the site of solubilization and absorption of LNCs. A digestive buffer prepared by calcium chloride, sodium hydroxide, tris maleate, taurocholic acid, alpha phosphatidylcholine, and sodium chloride were the ingredients for making lipolysis media, as demonstrated in Table 8. The prepared mixture simulates the fasted state of the gastro-intestinal tract (GIT). The buffer mentioned above solution was adjusted to pH-6.8 by adding 1M sodium hydroxide at 37 °C. The LNC formulations of ERVN-TPGS and digestive buffer were mixed to attain a concentration of 5 mg per mL, followed by adding 1.75 mL of pancreatin with continuous stirring for 30 minutes. Enzymatic digestion started by adding 0.15 M NaOH, and the pH was kept at 6.8 throughout the process. The experiment was conducted for half an hour. The addition of sodium hydroxide was recorded to maintain a pH of 6.8, and the liberation of fatty acids was estimated. After the completion of the experiment, the blend was centrifuged for 30 minutes to segregate the two layers. An aqueous phase (supernatant part) containing monoglycerides, fatty acids, and bile salt was used for

collection. The sediment part is also separable, containing lipid-based components such as di-glycerides, triglycerides, and insoluble fatty acids. The amount of ERVN was calculated in each layer, i.e., the aqueous layer and the lipidic layer [34].

2.3.11. *In-vitro* Haemolysis

A hemolysis study investigated the compatibility of ERVN-TPGS-loaded LNCs formulation with blood components. A blood specimen was obtained from Wistar rats into EDTA-filled tubes and centrifuged at 5000 rpm for 15 minutes (Animal Protocol No. 1706). Afterward, the supernatant was discarded after centrifugation. The sediment was rinsed thrice using a phosphate buffer solution (pH 7.4) [37]. The final sediment was further exposed to centrifugation for 15 minutes at 4000 rpm, the excess PBS was poured out, and the sediment mass was collected. Finally, 20 µL of ERVN-TPGS-loaded LNCs were added to the 96 well plates after 180 µL of the diluted sedimented sample.

Drug suspension, negative control (1% triton X 100), positive control (PBS), and LNCs placebo were added to the corresponding 96 well plates. After adding various samples to the blood sediment for 1 h, OD (optical density) was estimated at 570nm by the Elisa plate reader. The percentage of hemolysis was estimated using the following formula:

$$\% \, Haemolysis = \{\frac{(ODS - ODP)}{ODPS}\} \times 100$$

ODS, ODPS, and ODP represent the sample's optical density, positive control's optical density, and placebo's optical density, respectively.

2.3.12. Stability study in simulated gastric fluid (SGF)

SGF was formed using 0.7% hydrochloric acid (HCl), 0.2%w/v of sodium chloride, and 3.2 mg/mL of pepsin and maintained a pH of 1.2 of the media. Further, as reported by Khan and coworkers, SGF media, fasted-state simulated intestinal fluid (FaSSIF) media, and fed-state simulated intestinal fluid (FeSSIF) media were prepared and used to examine stable nanoformulations [38]. The experiment was performed with continuous stirring (100 rpm) at 37 ± 0.5°C. The samples were taken out regularly, and globule size and PDI were evaluated.

2.3.13. Gut sac permeability study

The intestine gut of an overnight fasted rat was used to investigate gut permeability (IEAC, Jamia Hamdard Protocol No. 1706). The Wistar rat was sacrificed by CO_2 inhalation, and their intestinal guts were removed and cleaned with a tyrode solution pH-7.4. 3mL of ERVN-TPGS-LNCs were filled using a disposable syringe, and the ends of the intestinal gut were knotted to create a sac-like structure. Then, the intestinal bag was kept in 100 mL of aerated tyrode buffer solution maintained at 37°C. 2 mL of the aliquot was taken out at 5 minutes, 15 minutes, 0.5h, 1h, and 2h. The exact amount of tyrode solution was added to keep the sink in condition. The same procedure was applied for the ERVN-LNCs and ERVN-S, and the amounts of the drug were determined using UV spectroscopy. The formula was used to compute the flow and apparent drug coefficient [39].

$$Flux\ of\ drug\ (J\ in\ \mu g/cm^2/min) = \frac{Conc(\mu g/mL) \times Dilution\ factor \times Volume\ of\ medium(mL)}{Permeation\ area\ (cm^2)}$$

$$Apparent\ Permeation\ Coefficient\ (P)\ in \frac{cm}{minute} = \frac{J}{Co}$$

C_0 indicates the initial quantity of ERVN added in the donor compartment.

2.3.14. Examination of intestinal depth permeation using confocal laser scanning microscopy (CLSM)

The small intestine was cut into 5–6 cm long sections, and the discharged waste was removed using a tyrode solution. Rhodamine B tagged with ERVN-LNCs, ERVN-TPGS-LNCs, and ERVN-S was filled in the tied intestine at one end, followed by knotting at the other to create a sac-like structure. Then, the ERVN-loaded LNCs, ERVN-TPGS-LNCs, and ERVN-S were filled in intestinal lumen and kept for 2 h in tyrode buffer solution at 37 ± 0.5 ˚C with stirring at 100 rpm and supplied with aeration from an aerator. After the treatment, the intestine was incised and washed with tyrode buffer solution to remove different stains from the intestine. A slice of the small intestine was stained on the clean glass slide to evaluate permeation studies. The depth of the permeation of ERVN from ERVN-LNCs and ERVN-TPGS-LNCs formulation and ERVN-S across the intestine section were examined through the z-axis of a confocal microscope (LEICA TCS SPEII Leica Microsystem Ltd., Germany) with LAS AF software [31].

2.4.*In-vivo* - Pharmacokinetic (Pk) analysis

All the tests on Wistar rats were performed as per recommended regulations by Institutional Animal Ethical Committee (IAEC Protocol No. 1706, Jamia Hamdard). All the animals were taken care of as prescribed by the guidelines for standard laboratory care and food. The Pk investigation was conducted in wistar rats, which were divided into three groups. One set of Group (group A) represents ERVN-S with 0.25%w/v sodium carboxymethyl as a suspending agent, and another set of groups represents ERVN-TPGS-LNCs and ERVN-TPGS-LNCs + CYHD as shown in Table 2. The dose of ERVN for rats was calculated as the below formula.

$$Human\ Equivalent\ Dose\left(\frac{mg}{kg}\right) = Animal\ dose\ (\frac{mg}{kg}) \times \frac{Animal\ Km}{Human\ Km}$$

For wistar rats, the correction factor (Km) is equal to 6, and for humans, it is 37. The Km is estimated by dividing the mean body weight of a species by its body surface (m^2).

After administering the samples to rats, the blood samples were collected at intervals of 0.5, 1, 2, 4, 8, 12, 24, and 48 h. The collected blood samples were supposed to be centrifuged for 40 minutes at 3000 rpm, and the plasma was isolated from the supernatant. The plasma was kept for refrigeration at -80 °C until further examination. Then, the plasma samples were thawed and mixed with acetonitrile to deproteinize the sample. The sample was centrifuged for 30 minutes at 3000 rpm to decant the protein in the plasma. The supernatant was collected to estimate the drug content in the sample using an HPLC instrument [30].

2.5.Chylomicron blockage model for a confirmatory test of the lymphatic uptake of ERVN-TPGS-LNCs

This study was performed per the guidelines approved by the IAEC Protocol No. 1706 of Jamia Hamdard, New Delhi, India. A single oral dose of ERVN-TPGS-LNCs was given to the Wistar rat after cycloheximide (CYHD). Using a feeding needle, animals were orally administered lipidic-based nanocarrier (ERVN-TPGS-LNCs) at an equivalent 8.8 mg/kg body weight dose. The group was first given an i.p. injection of CYHD solution (3mg/mL) in normal saline before one hour of administration of ERVN-TPGS-LNCs. CYHD is a chylomicron blocker that prevents the entry of ERVN into the lymphatic pathway, as shown in Table 1 [40]. The blood was collected and estimated using the same method as described in pharmacokinetic study.

Table1. A grouping for pharmacokinetic profiling and chylomicron flow blocker.

Group (n=6)	Route and dose
ERVN-S	p.o, 8.8mg/Kg ERVN dispersed in 0.25% w/v of sodium carboxymethyl cellulose.

ERVN-LNCs	p.o, 8.8mg/Kg ERVN-LNCs dispersed normal saline.
ERVN-TPGS-LNCs	p.o, 8.8mg/Kg ERVN-TPGS-LNCs dispersed normal saline.
ERVN-TPGS-LNCs + CYHD	p.o, 8.8mg/Kg of ERVN-TPGS-LNCs dispersed in normal saline after the CYHD (3mg/Kg) treatment.

2.6.Statistical analysis

The data were statistically analyzed using GraphPad Prism 9.0 (Graph Pad, Unites States). All the data were shown as mean and standard deviation (mean ± SD). For the analysis of the data, Dunnett comparison experiment was performed for one-way ANOVA. The statistical significance was determined at $p < 0.05$.

3. RESULTS AND DISCUSSION

3.5.Selection of liquid and solid lipids

ERVN demonstrated the maximum solubility in Gelucire 44/14 (12.54 ± 1.179 mg/g) among solid lipids. Lipids could be because of their inherent self-emulsifying attribute, which assists in increasing the aqueous solubility in order to enhance the oral bioavailability of the ERVN. Furthermore, the higher carbon content may improve the ability to solubilize hydrophobic drugs. However, Precirol ATO 5 (3.23 ± 0.869) mg/g was selected to fabricate LNC formulations because Gelucire could not make stable nanocarrier systems [41]. Among the oils, ERVN demonstrated higher solubility in Labrafil M-2125CS (32.787 ± 3.978 mg/mL). Labrafil M-2125CS acts as a water-insoluble lipid and enhances the bioavailability of ERVN. Chemically, Labrafil M-2125CS, a long-chain triglyceride, showed more solubility than the medium-chain lipids as a result of enhanced entrapment of ERVN, as shown in fig 2 [41].

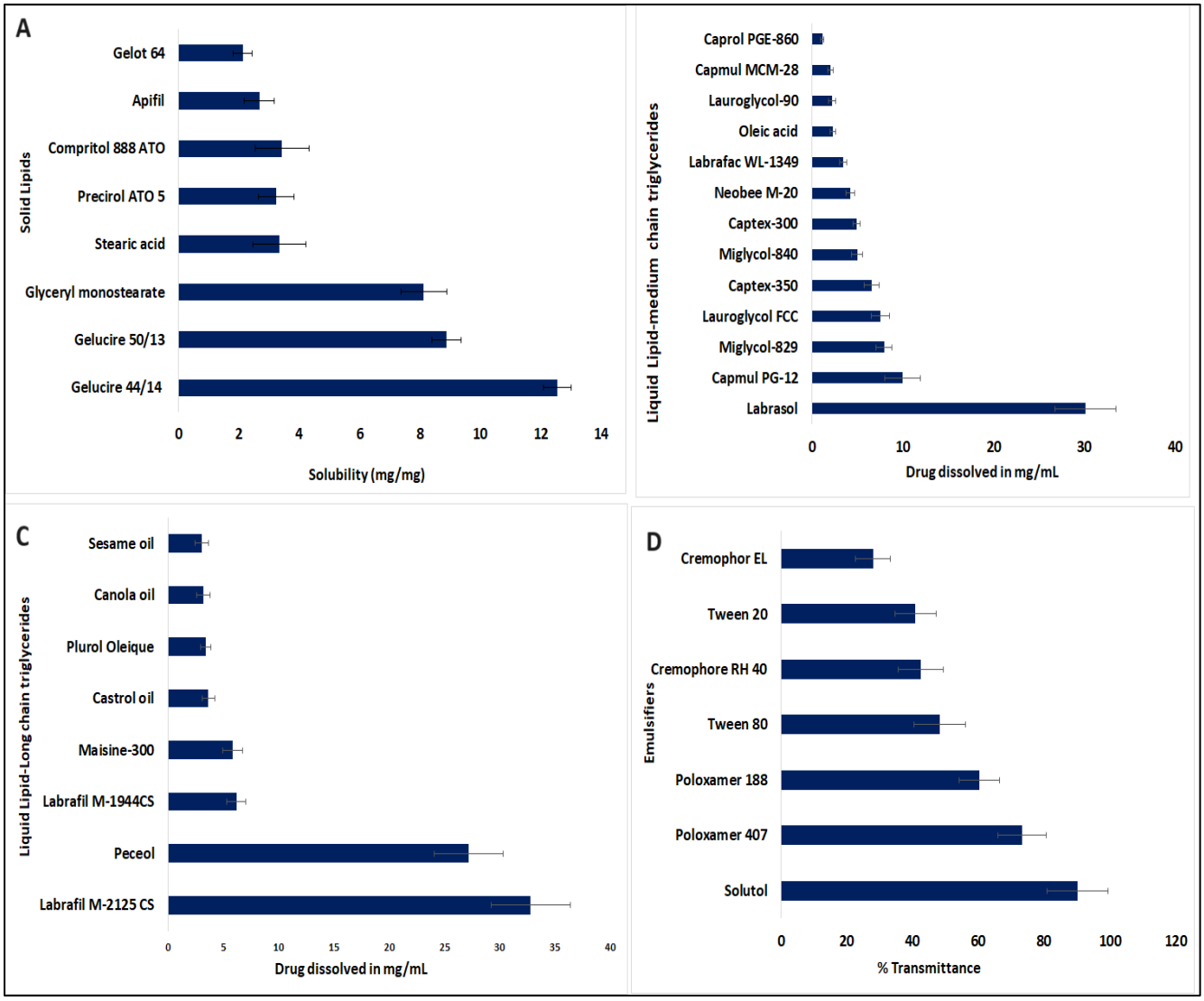

Fig 2. Solubility of ERVN in different (A) solid lipids, (B) medium chain liquid lipids (C) long chain liquid lipids, and (D) transmittance of emulsifier. The solubility of ERVN was demonstrated in Precirol ATO 5 (3.23 ± 0.869) mg/g), Labrafil M-2125 CS (32.787 ± 3.978 mg/mL) and Solutol H-15 (% transmittance of 90.22 ± 9.23). Data represented as (Mean ± SD).

3.6.Selection of Binary lipid mixture

Multiple proportions of Precirol ATO 5 and Labrafil M-2125CS were tested (90:10, 80:20, 70:30, 60:40, 50:50, and 40:60) to estimate their compatibility. The proportion of 40:60 did not exhibit any phase segregation, even after keeping it for 72 h, although all other ratios were separated after 24 h [3]. Therefore, this selected proportion was observed to the high %EE of ERVN and its ability

to maintain the semi-solid texture at 25 ± 1˚C. A higher amount of liquid lipid in a mixture indicates higher drug loading due to the higher solubility of ERVN in liquid than solid lipid. Further, increasing the concentration of liquid lipids causes a reduction in globule size, which leads to a decrease in viscosity and surface tension [30].

3.7.Thermal examination of a binary lipid mixture by DSC

In a binary lipid mixture, as the % of Labrafil M-2125CS (liquid lipid) by addition of 10%, the enthalpy for the melting point drops with respect to Precirol ATO 5 (100% of solid lipid), as represented in Fig 2. Even so, the crystallinity index (CI) is less variable in the proportion of 6:4 to 4:6 than to 7:3 to 9:1. As a result, the final ratio of the binary mixture was chosen, i.e., 4:6, as represented in Fig 3. Rojekar and associates stated a similar ratio for a suitable BM, i.e., solid and liquid lipids [3].

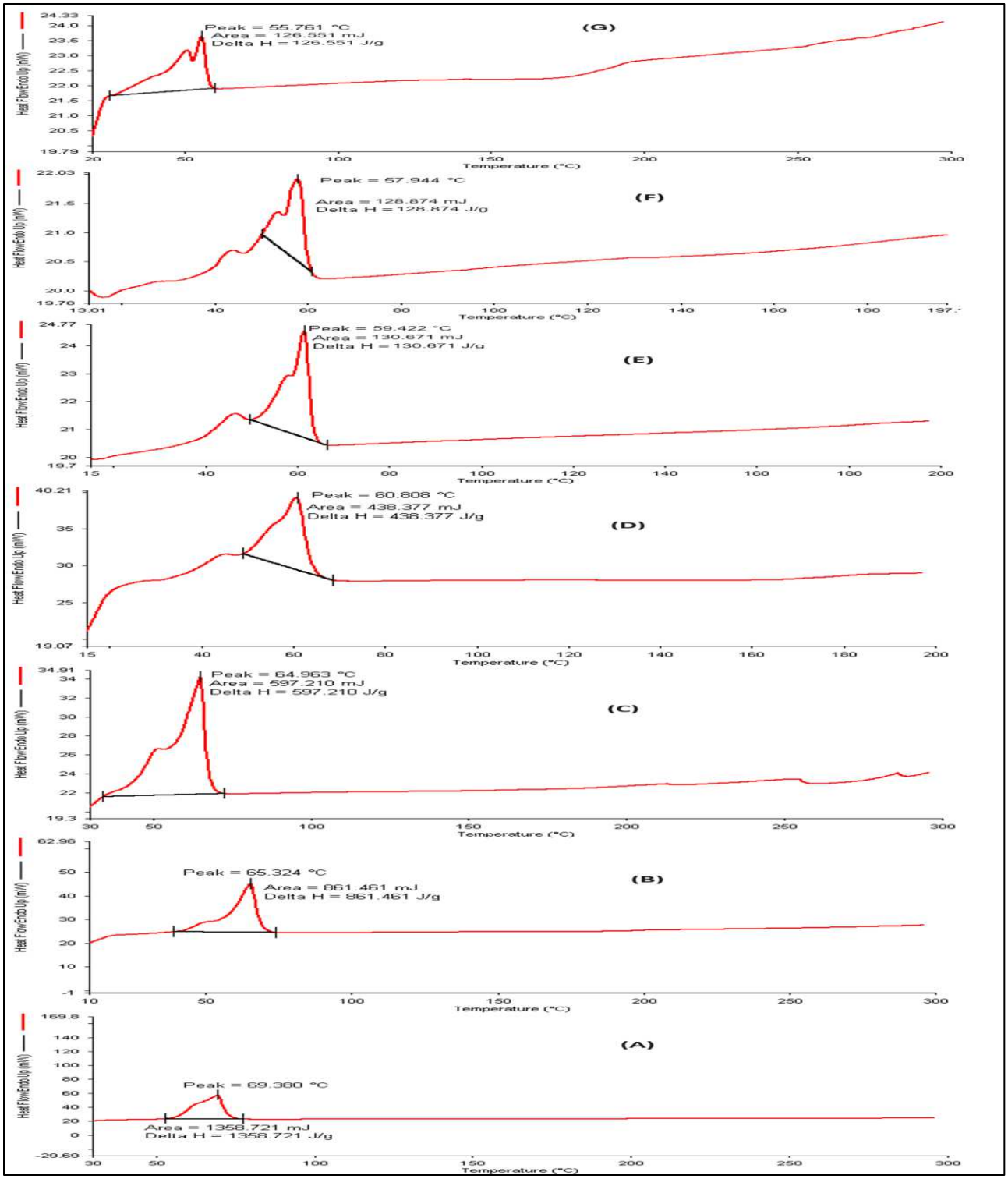

Fig 3. DSC Thermogram showed (A) Precirol ATO 5- 100% w/w, (B) BM with 90% Precirol ATO 5, (C) BM with 80% Precirol ATO 5, (D) BM with 70% Precirol ATO 5, (E) BM with 60% Precirol ATO 5 (F) BM with 50% Precirol ATO 5 (G) BM with 40% Precirol ATO 5.

3.8.Surfactant selection

The figure shows that a binary mixture with several surfactants was evaluated because % transmittance is related to emulsification property and particle size. The binary mixture (Precirol ATO 5 and Labrafil M-2125CS) exhibited a higher transmittance with Solutol H 15 (acts as a surfactant). Alam and associates fabricated isradipine nanostructured lipid carriers. Their research reported that the surfactant selection was based on the percentage transmittance estimated by UV spectroscopy at 510 nm. In addition, the surfactant selection was also evaluated based on PDI, particle size, and the percentage entrapment efficiency of the nanocarrier system. 1% of the surfactants were selected based on their lowest solubility. From the list of screened surfactants, poloxamer 407 and tween 80 showed 73.24 ± 1.28 and 48.21 ± 0.135 % of transmittance, respectively, as shown in fig 1 [23].

Further, the particle size and PDI of poloxamer 407 and tween 80 also showed 783.32 ± 4.35 nm, 0.867 ± 0.045, and 985 ± 5.74 nm, 0.432 ± 0.043, respectively, showing a heterogenous and broad particle size distribution. Also, the binary mixture was incompatible with poloxamer 407 or tween 80. Therefore, it was not taken further for optimization of lipid-based nanocarriers.

On the other side, Solutol H-15 exhibited a small globule size and PDI value. Due to the compatibility of Solutol H-15 with binary mixtures and its higher HLB value of 16 (CMC concentration of 0.005%-0.02%), this could be the reason for its small globule size and homogeneous globule distribution. It can also stabilize steric with its exceptional solubilizing property and intrinsic amphiphilicity due to the hydro-steric acid and ethylene-oxide. Therefore, Solutol H-15, a non-ionic surfactant, is generally considered safe for human ingestion and has low toxicity. Furthermore, it also functions as a potent p-glycoprotein inhibitor and penetration enhancer. As a result, it enhances the hydrophilicity, diffusion, and dissolution of the drug in the

gastro-intestinal tract. It inhibits the p-gp efflux pump, which leads to enhanced absorption of the drug [23].

3.9.Selection of TPGS concentration

For the optimization of TPGS concentration, various concentrations of stabilizers were screened by visual observation, phase separation, and percentage transmittance in the dispersion medium. Smaller and more uniform globules in the dispersion medium showed a higher percent transmittance, which indicates stable nanoformulation, as shown in Table 2. However, TPGS could also increase particle size due to Ostwald's ripening, as reported by Malamatari and associates [42]. Thus, the findings demonstrated that ERVN-loaded LNCs with TPGS (0.1% w/w) were more homogenous and stable than those without TPGS loading formulation.

Table 2. Optimization of Vitamin E-TPGS concentration in LNCs using 2% BM, 180 seconds sonication time, and 1.5% Surfactant (Mean ± SD, n=3).

Parameters	Vitamin E TPGS concentration			
	0.01%w/w	**0.1%w/w**	**0.5%w/w**	**1%w/w**
Optical clarity	Transparent and clear	Transparent and clear	Transparent and clear	Opaque and Turbid
Phase separation after 1 month	No Phase separation	No Phase separation	No Phase separation	Phase separation
%T (Mean ± SD)	89.67 ± 0.75	97.22 ± 1.08	96.54 ± 0.99	91.04 ± 1.53
Mean particle size ± SD nm after 48h	107 ± 0.117	138.28 ± 0.165	192.7 ± 0.245	276.2 ± 0.209
PDI (Mean ± SD) after 48h	0.422 ± 0.091	0.174 ± 0.043	0.452 ± 0.011	0.621 ± 0.087
Zeta potential (Mean ± SD) mV after 48h	-2.76 ± 0.187	-7.34 ± 0.119	-2.46 ± 0.432	-5.89 ± 0.339
%EE (Mean ± SD)	94.21 ± 1.89	95.49 ± 1.26	97.34 ± 1.22	97.94 ± 1.29

3.10. Optimization of NLCs using CCD

The pharmaceutical formulation should be optimized to meet the desired formulation performance concerning the quality of the formulation (QoF), which is commonly associated with justified process parameters, and efficacy of formulation, which is known as the quality target of the product profile (QTPP), as shown in Table 3. The main idea of presetting the QTPP was to create patient-driven ERVN-TPGS-LNC formulations where the formulation could provide the maximum therapeutic benefit to the subject, as shown in Table 4. The dependent factors such as globule size, Polydispersity index, and %EE are regarded as the critical quality attributes (CQAs) of the formulation, as shown in Table 5. The major parameters further evaluated for optimization of LNCs using CCRD from initial experimental data were binary lipid conc. (1–2% w/w), emulsifier conc. (0.5–1.5% w/w), and sonication time (60–180 seconds). For risk assessment, which involved quantitative and qualitative assessment, an Ishikawa fishbone diagram was prepared to determine the critical material attributes and process attributes that influence the fabrication of nanoformulation, as shown in Fig 4.

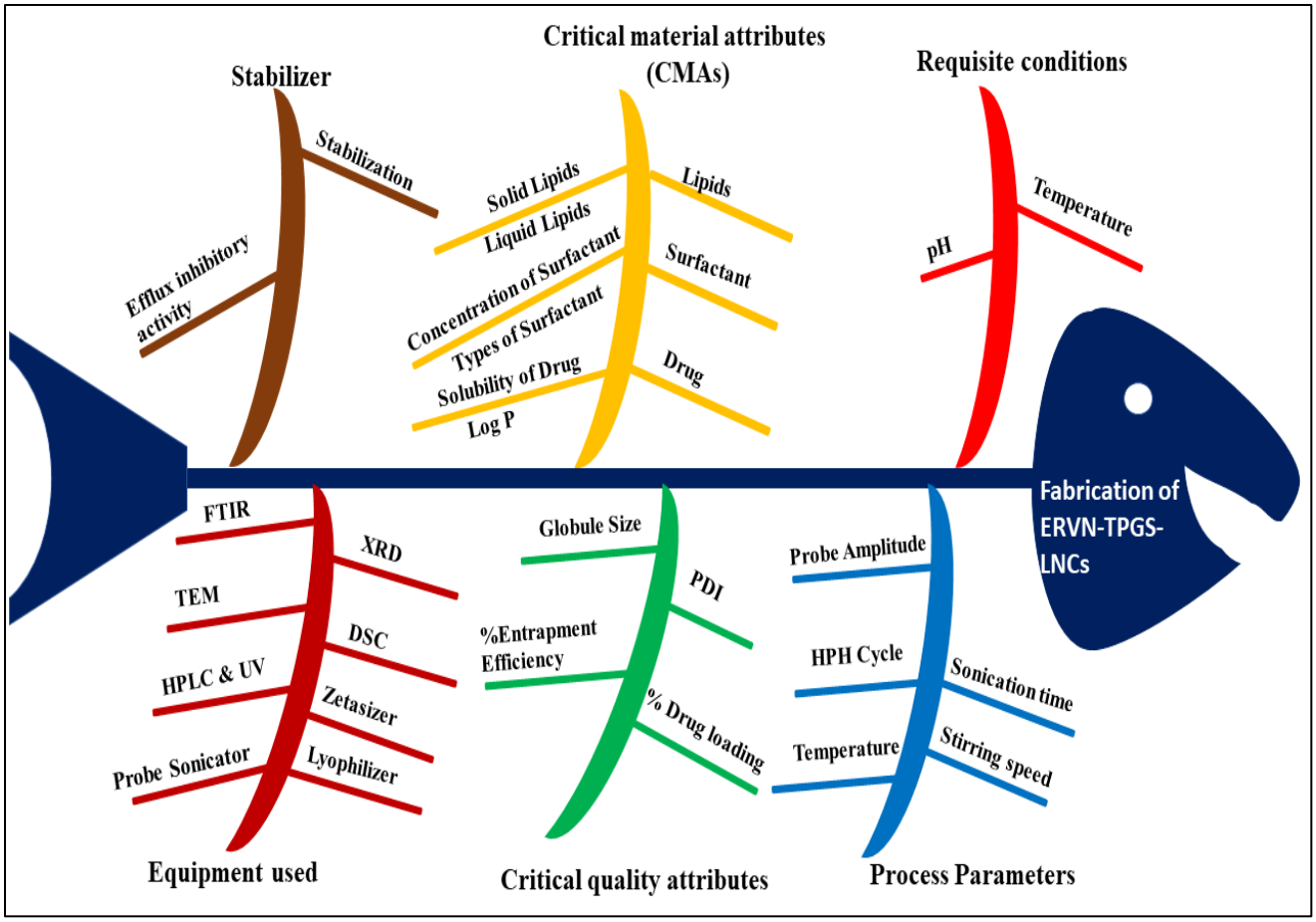

Fig 4. Ishikawa fishbone diagram for various variables.

The CCRD was applied to investigate the impact of the independent variables on the responses, including globule size, PDI, and %EE. The applied design created 20 experimental runs, as shown in Table 5. As per the recommended runs, all the trials were fabricated and evaluated to estimate the influences of the independent factors, i.e., the conc. of the binary lipid mixture (%), the concentration of the surfactant (%), and probe sonication time (seconds) on the dependent factors, i.e., the globule size in nm, the PDI, and % EE. The responses of the trials are shown in Table 5.

Table 3. Quality target of product profile (QTPP) of the LNCs.

QTPP Variables	Target formulation	Remarks
Dosage	Lipid nanocarrier system	It improves the drug permeation and bioavailability.
Administration route	Oral	The simplest route is bypassing hepatic metabolism via lymphatic uptake, which results in the maximum amount of drugs available for therapeutic action.
Physical form	Freeze-dried powder	It can be administrated easily
Characterization of nanoformulation	Globule size, PDI, %EE.	It can affect the permeation and absorption.
Pharmacokinetics (PK)	Targeting and metabolism	To achieve optimal therapeutic efficacy.

Table 4. Levels and Variables applied in Central composite rotatable design (CCRD) i.e., independent variables (Binary mixture, Surfactant concentration, and probe sonication time) and dependent variables (particle size, PDI, and % Entrapment efficiency).

Independent factors	Levels				
	Axial -α	**low (-1)**	**medium (0)**	**high (+1)**	**Axial +α**
A- Binary lipid concentration (%w/w)	0.6591	1	1.5	2	2.3409
B- Surfactant concentration (%w/w)	0.1591	0.5	1	1.5	1.8409
D- Probe sonication time (second)	19.092	60	120	180	220.908
Dependent factors					
R1 - Globule size (nm)	Minimum				
R2 - Polydispersity Index	Minimum				
R3 - Entrapment Efficiency (%)	Maximum				

Table 5. Enumerate several critical quality attributes (CQAs) influencing the effectiveness of ERVN-LNCs as a treatment option.

CQA variables	Target	Remarks
Globule size	80.00-200.00 nm	This size assures absorption, thus improving bioavailability.

%EE	>60.00%	To attain the desired therapeutic concentration.
PDI	<0.5	homogenous distribution of the particle.

3.11. Evaluation of responses

3.11.1. Globule size

The average particle size after formulating twenty runs was between 25.67 and 657.37nm. The below quadratic equation exhibited a remarkable impact of the binary lipid mixture, emulsifier, and probe sonication time on the PDI and globule size, as shown in fig 5 (A). It was interpreted that the percentage of a binary mixture, emulsifier, and sonication is significant ($p < 0.0001$) in globule size. In addition, it was also observed that using a lower binary mixture, the resulting globule size was in the range of 25.67 and 338.58 nm. However, a higher percentage of the binary mixture formed globules whose sizes varied from 89.58 to 589.51 nm. Therefore, a medium percentage of the binary mixture produced optimal globule size in the formulation, as shown in Table 6.

$$R1 = 122.57 + 157.30A - 83.61B - 70.16C + 4.81AB + 4.02AC + 67.18BC + 74.36A^2 + 53.72B^2 + 28.55C^2$$

Further, increasing the percentage of surfactant reduced the surface tension between the lipidic and aqueous phases, leading to smaller globules. The smaller globule may have been formulated by breaking the larger globule into the smaller globule [25]. Thus, sonication time also had a notable impact on the particle size of the formulation. Additionally, prolonging the sonication period above 120 seconds converts stable globules to agglomerating globules and growing globule size [43]. The figure shows the corroborated impact of independent factors on globule size, such as the negative effect of the percentage of a binary mixture and surfactant concentration (AB) and the

positive impact of the percentage binary lipid mixture and sonication time (AC), and also a positive effect of percentage of surfactant and sonication time concentration (BC).

Table 6. Central composite rotatable design (CCRD) shows the experimental trails for the three variables with responses acquired after performing the respective trails.

Run	Binary mixture (%)	Surfactant (%)	Sonication time (seconds)	Globule size (nm)	PDI	%EE
1	1.5	1	120	123.33	0.171	93.96
2	0.659104	1	120	25.67	0.584	42.58
3	2.3409	1	120	589.51	0.743	97.35
4	1	1.5	60	79.85	0.475	52.47
5	1.5	1	120	125.32	0.173	94.32
6	2	1.5	60	344.98	0.673	96.34
7	1	0.5	180	116.39	0.422	65.38
8	2	0.5	60	657.37	0.632	97.96
9	1.5	1	120	123.91	0.172	94.12
10	1	0.5	60	338.58	0.499	66.35
11	1.5	1	120	123.68	0.172	93.98
12	1.5	0.159104	120	408.85	0.496	90.76
13	1.5	1	120	120.43	0.171	94.47
14	1.5	1.8409	120	89.58	0.538	79.35
15	1.5	1	220.908	31.38	0.382	87.45
16	2	1.5	180	407.58	0.635	93.54
17	1	1.5	180	53.48	0.403	53.57
18	1.5	1	120	127.43	0.173	94.11
19	2	0.5	180	378.39	0.567	89.67
20	1.5	1	19.0924	324.67	0.366	82.53

3.11.2. PDI

PDI represents the uniform distribution of globules in the LNCs formulation. The average PDI values for all trails range from 0.171 to 0.743. A significant impact of lipid conc. ($p < 0.0001$), surfactant conc. ($p > 0.2720$), and probe sonication time ($p = 0.0845$) on PDI was shown in fig 5 (B). The following equation showed that the PDI value was directly proportional to an increase in

lipid concentration. In contrast, it was inversely proportional to the concentration of surfactant and sonication time. Nevertheless, the addition of surfactant helped offer stabilization by steric effect due to the formulation consisting of a dense hydrophobic tail that did not allow the globule to come closer to forming a large globule [23].

$$R2 = +0.1720 + 0.0714A + 0.0100B - 0.0165C + 0.0190AB + 0.0058AC + 0.0040BC + 0.1736A^2 + 0.1218B^2 + 0.0712C^2$$

The above equation also recommended that the globule size be reduced with an increase in sonication time, thereby preventing them from making aggregation and hence keeping the nanocarriers stable with a reduced PDI value (PDI <0.5). However, it was observed that further increasing the sonication time resulted in the formation of clusters of globules, resulting in a non-uniform globule distribution. The 3D graphs displayed the amalgamed impact of two independent factors on the polydispersity index, which exhibited an increase in the conc. of the binary mixture and emulsifier elevated the Polydispersity index. On the other side, sonication time demonstrated a negative effect on PDI. However, the concentration of the binary mixture and surfactant (BC) positively affected PDI, as shown in Table 6.

Table 7. Statistical summary of responses.

Responses	Statistical model summary				Suggested Model	Significance value (p-value)		
	R^2	Adjusted R^2	Predicted R^2	Std Dev.		A	B	C
R1	0.9788	0.9596	0.833	37.63	Quadratic	<0.0001	<0.0001	<0.0001
R2	0.9858	0.973	0.8913	0.0318	Quadratic	<0.0001	0.272	0.0845
R3	0.9912	0.9833	0.933	2.23	Quadratic	<0.0001	0.0004	0.7508

3.11.2.1. Entrapment Efficiency

The percentage EE percentage of all the runs was between 42.58 and 97.96%. Table 6 showed that EE was significantly impacted by binary mixture ($p < 0.0001$) followed by the percentage of surfactant ($p=0.0004$) and probe sonication time ($p=0.7508$). As per the below-mentioned statistical equation, the increment in the percentage of the binary mixture increased the % EE as the percentage of the binary mixture improved the solubility of the ERVN because of the collection of the drug into the void spaces of the imperfect binary mixture as shown in fig 5 (C). Furthermore, % EE improved by adding a small amount of surfactant due to forming a multilayer surfactant film around the globule, which provided additional space for drug incorporation. It also employs the surfactant to improve the solubilization of the insoluble drug by incorporating it into the lipid matrix system [41, 43].

$$R3 = + 94.23 + 16.98A - 3.12B - 0.1966C + 3.49AB - 1.40AC + 0.9450BC - 9.03A^2 - 3.69B^2 - 3.71C^2$$

An interaction of independent factors such as surfactant conc. and lipid conc. (AB); and surfactant concentration and sonication time (BC) demonstrated a positive impact, although the correlation of a binary lipid mixture and sonication time (AC) had a negative impact, as shown in Table 5.

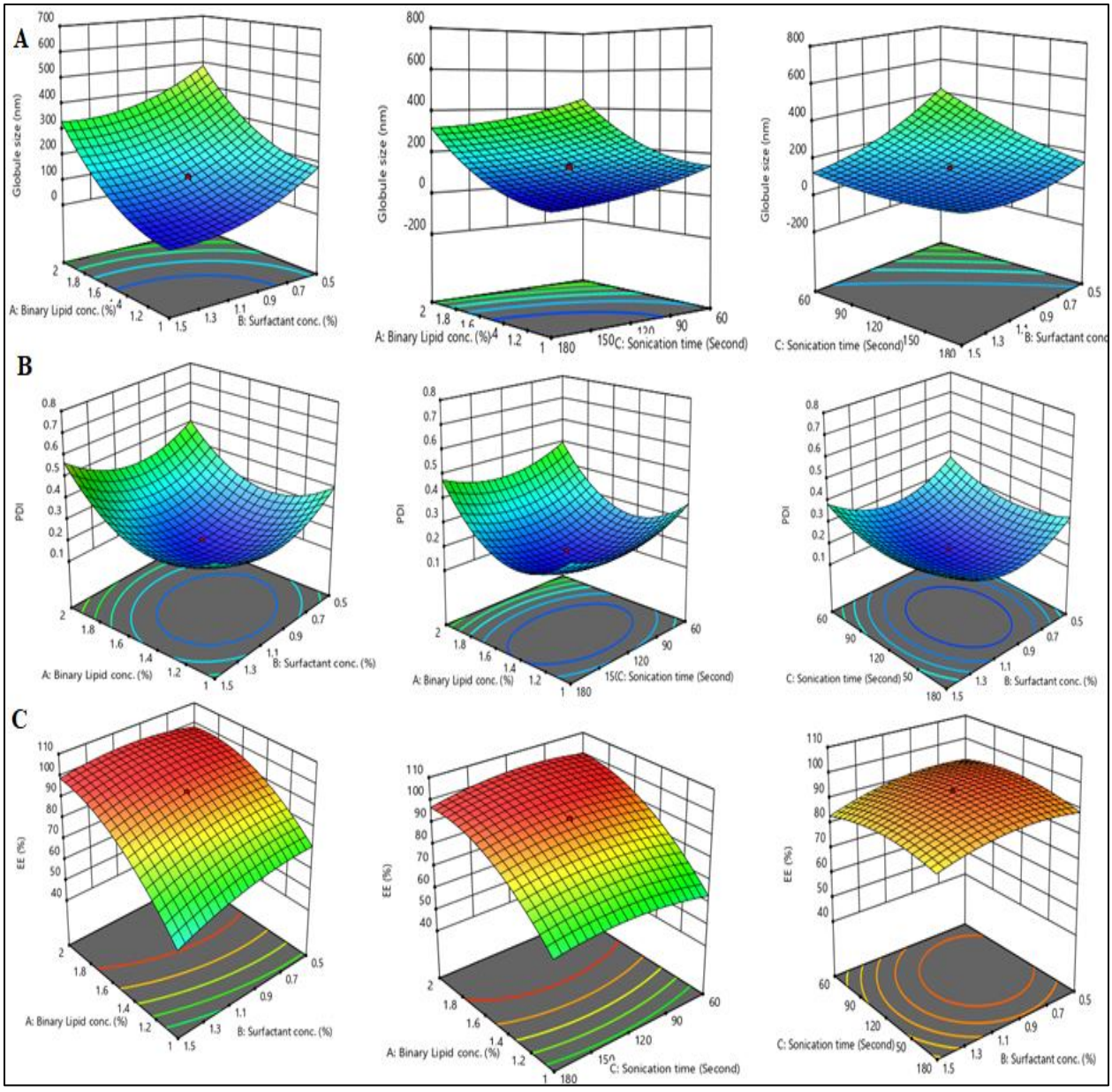

Fig 5. A 3D response graph represents the effect of binary mixture (%), sonication time (seconds), and surfactant concentration (%) on (A) globule size; (B) PDI; and (C) %EE.

3.11.4. Validation of optimization

A central composite rotatable design was used to attain an ideal nanoformulation with minimum globule size, Polydispersity index, and a maximum percentage of EE. The statistical tool obtained the predicted values of all the dependent variables in Table 7. Thus, EVRN-TPGS-LNCs were

fabricated depending on the number of process variables, runs, and their responses, as represented in Table 7. Further, the experimental outcomes collected from the nanoformulations were compared to the expected response. The experimental and expected values were found to be nearly identical, which indicates the validity of the design. Furthermore, the desirability responses were close to 1, showing very low prediction error compared to desirability values for responses.

3.11.5. Optimized formula

The finalized ERVN-TPGS loaded LNCs from CCRD were prepared by adding a binary mixture (1.5% w/w), emulsifier (1% w/w), and sonication time of 120 seconds. The finalized formula was again characteristic of several other parameters.

3.12. Characterization of optimized formulation

3.12.4. Globule size and PDI

To prepare a nanoformulation with gelucire 44/14 and glyceryl monostearate as solid lipids, these solid lipids formed a creamy solution that showed rapid segregation of solid lipids. However, it was observed that the formulation was not even stable for 2 h, as precipitation was exhibited.

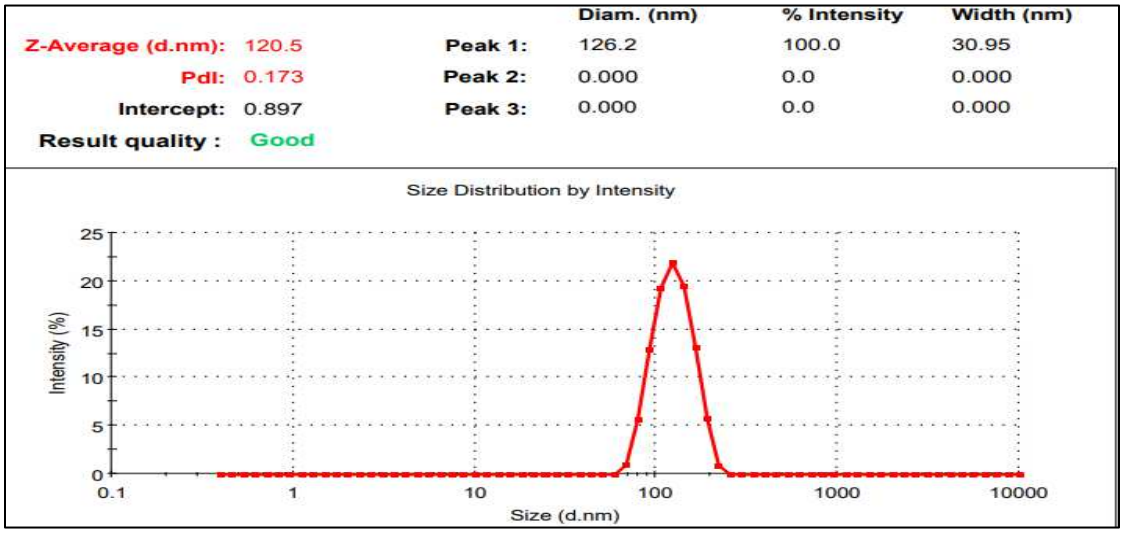

Fig 6. Globule size and PDI of ERVN-TPGS loaded LNCs.

Although these solid lipids showed maximum solubility, these solid lipids could not proceed further for formulation development. On the other side, Compritol 888 ATO exhibited slow sedimentation that would allow globules to grow and form large globules. Furthermore, Precirol ATO 5, which has higher partitioning and miscibility with ERVN, would have fabricated stable lipid-based nanocarriers; therefore, Precirol ATO5 was taken forward for optimization of LNCs formulation.

ERVN-TPGS-LNCs were designed with Precirol ATO 5, which has polydisperse globule sizes (60–300 nm) with an average globule size (120.56 ± 2.174 nm) and a broad polydispersity index (0.173 ± 0.042) with exceptional colloidal stability as shown in fig 6. The smaller globule size was attributed to the proper selection of surfactant and stabilizer. They decreased the surface tension by getting absorbed on lipid-water interfaces by creating a stable, packed surfactant layer.

The globule size is a critical outcome for the oral delivery of ERVN. Smaller globules contribute to a vast surface area and allow maximum penetration of the therapeutic molecules across the intestinal gut [3]. The result is more drug release from lipid-based nanocarriers, which can improve bioavailability in the brain and other organs. The polydispersity index (PDI) varies from zero (uniformly dispersed sample) to 1.0 (a highly heterogeneous sample). The findings resonated with previous literature, revealing that LNCs with small globule sizes and low PDI can freely enter the viral reservoir site [44].

3.12.5. %EE and %DL

The % EE and % DL of ERVN-TPGS-loaded LNCs were found to be 94.42 ± 4.65 and 8.94 ± 0.759, respectively. The lipophilic nature of ERVN could have led to partitioning into the binary lipid matrix, which could result in high entrapment efficiency. Further, increased entrapment

efficiency is based on increased binary mixture and surfactant. The globule of nanoformulation is surrounded by multiple layers of surfactant, which also helps to create enormous voids that can entrap as many drug molecules as possible. As a result, the entrapment efficiency and drug loading were improved [41].

3.12.6. Zeta potential

Zeta potential (ZP) is a tool that shows the stability of nanoformulation. ZP of the optimized ERVN-TPGS-LNCs was found to be -7.32 ± 0.021 mV, as shown in fig 7. A lower value of ZP represents the excellent scattering of the charged lipid particle that inhibits the globules, flocculation, coagulation, and aggregation [30].

Name	Mean	Standard Deviation	RSD	Minimum	Maximum
Zeta Potential (mV)	-7.185	-	-	-7.185	-7.185
Zeta Peak 1 Mean (mV)	-7.185	-	-	-7.185	-7.185
Conductivity (mS/cm)	0.09046	-	-	0.09046	0.09046
Wall Zeta Potential (mV)	-3.449	-	-	-3.449	-3.449
Zeta Deviation (mV)	5.846	-	-	5.846	5.846
Derived Mean Count Rate (kcps)	2.345E+04	-	-	2.345E+04	2.345E+04
Reference Beam Count Rate (kcps)	1789	-	-	1789	1789
Quality Factor	1.48	-	-	1.48	1.48

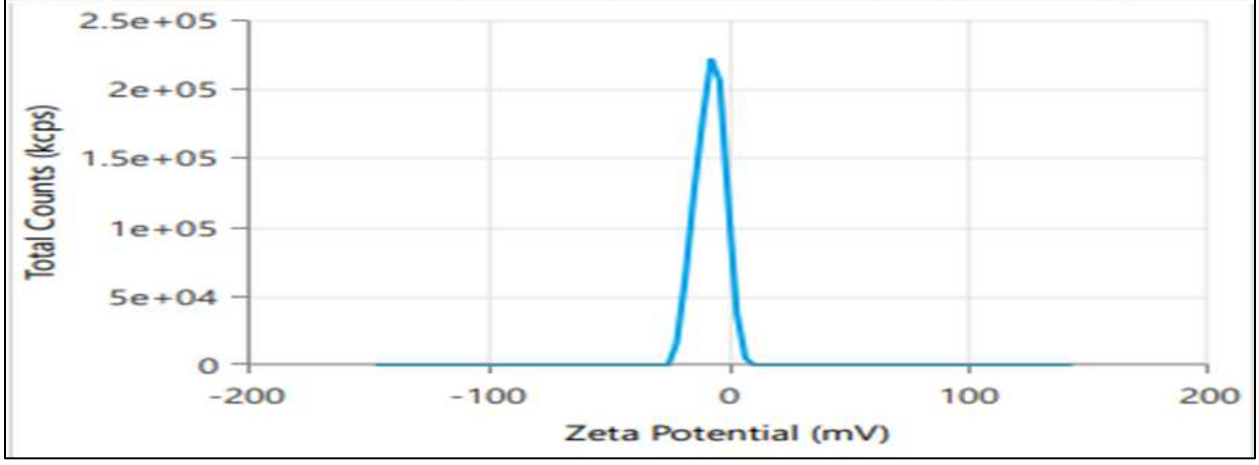

Fig 7. Zeta potential of ERVN-TPGS loaded LNCs.

3.12.7. Surface morphology by TEM

TEM figures were obtained to get more information regarding the morphology of the ERVN-TPGS-LNCs, particularly the surface and shape of the LNCs. As shown in fig. 8, the TEM images of the ERVN-TPGS-LNCs revealed a range of globule sizes of 80–300 nm and were seen as spherical. The shape of the globule could be because of the slow cooling of dispersed oil globules in the dispersed medium, resulting in the fabrication of spherical-shaped globules. Furthermore, the gentle congealing of the solid lipid in the melted binary mixture prepares an appropriate morphology of LNCs due to the crystalline attributes of solid lipids [30, 45]. The TEM images exhibited that ERVN-TPGS-LNCs were observed to be spherical and did not demonstrate any coagulation or aggregation. Further, the retrieved globule size data was correlated with DLS data.

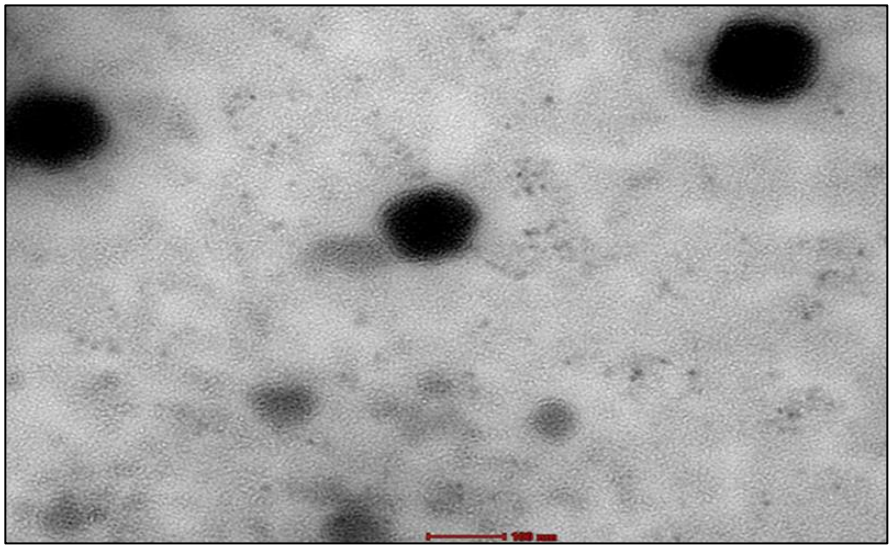

Fig 8. Surface morphology study by Transmission electron microscope. The scale bar showed 100 nm.

3.12.8. Powder X-Ray Diffraction (PXRD)

The optimized formulation of ERVN-TPGS-LNCs was freeze-dried to obtain freely flowing powder, and a PXRD examination was performed to characterize the solid state concerning the existence of a particular peak, as revealed in Figures 9A and 9B. The characteristic peaks of ERVN

were 9.27°, 19.51°, 23.63°, and 26.89°; two thetas denote the crystallinity of ERVN, and these specific peaks were employed to compare with the XRD of ERVN in ERVN-TPGS-loaded LNCs. The sharp characteristic peak of ERVN was missing in the ERVN-TPGS-loaded nanocarriers, indicating the absence of ERVN could be due to the encapsulation of ERVN inside the lipid matrix or might have changed it to an amorphous form. Sartaj and associates demonstrated the ribociclib-loaded NLC, where the specific peak of the ribociclib was absent in the XRD of drug-loaded nanocarriers, attributing ribociclib entrapped in nanocarriers [34].

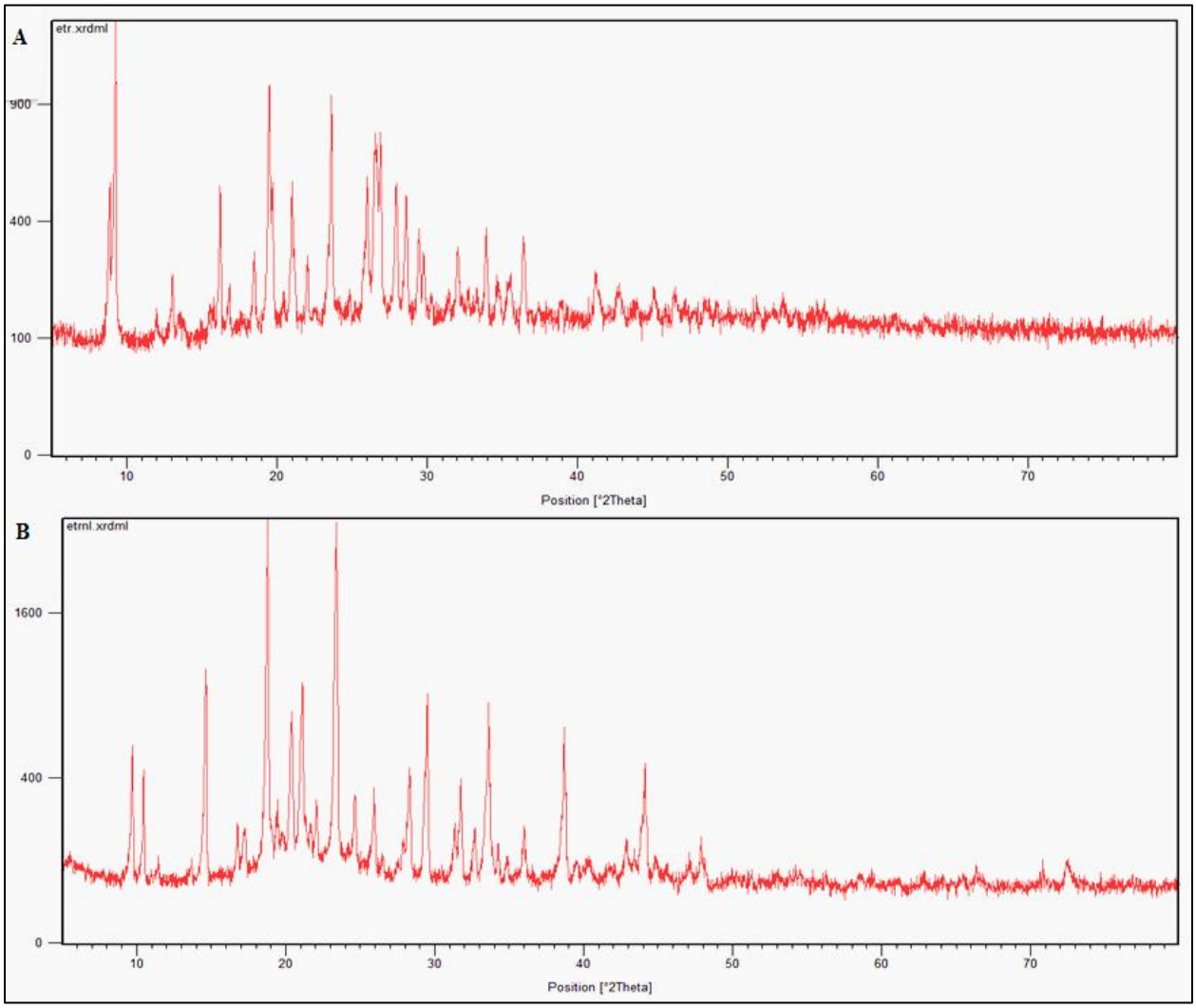

Fig. 9. P-XRD showed (A) ERVN and (B) lyophilized ERVN-TPGS-LNCs.

3.12.9. Structural analysis by FT-IR spectroscopy

The FT-IR examination has been performed for ERVN, placebo, and ERVN-TPGS-loaded LNCs, as shown in fig 10. The spectra of ERVN have been contrasted with placebo and ERVN-TPGS-loaded LNCs. The FT-IR spectra of ERVN-TPGS-loaded LNCs have shown the absence of 3410 cm^{-1} (stretching of primary aromatic amine), 2368 cm^{-1} (stretching of aryl C=N), 2978 cm^{-1} (aromatic C-H), 650 cm^{-1} (C-Br), 1365 cm^{-1} (primary and tertiary amine), and 1188 cm^{-1} (stretching of C-O-C), which confirmed the encapsulation of ERVN inside the lipid matrix. The chitosan-based nanoparticle was developed by Annu and associates, who stated that specific peaks of the drug, e.g., 3065 cm^{-1} (stretching of aromatic) and 3431 cm^{-1} (stretching of N-H), were absent in the nanoformulation when compared to the pure drug. It could be a probable reason for drug encapsulation within the polymer [46].

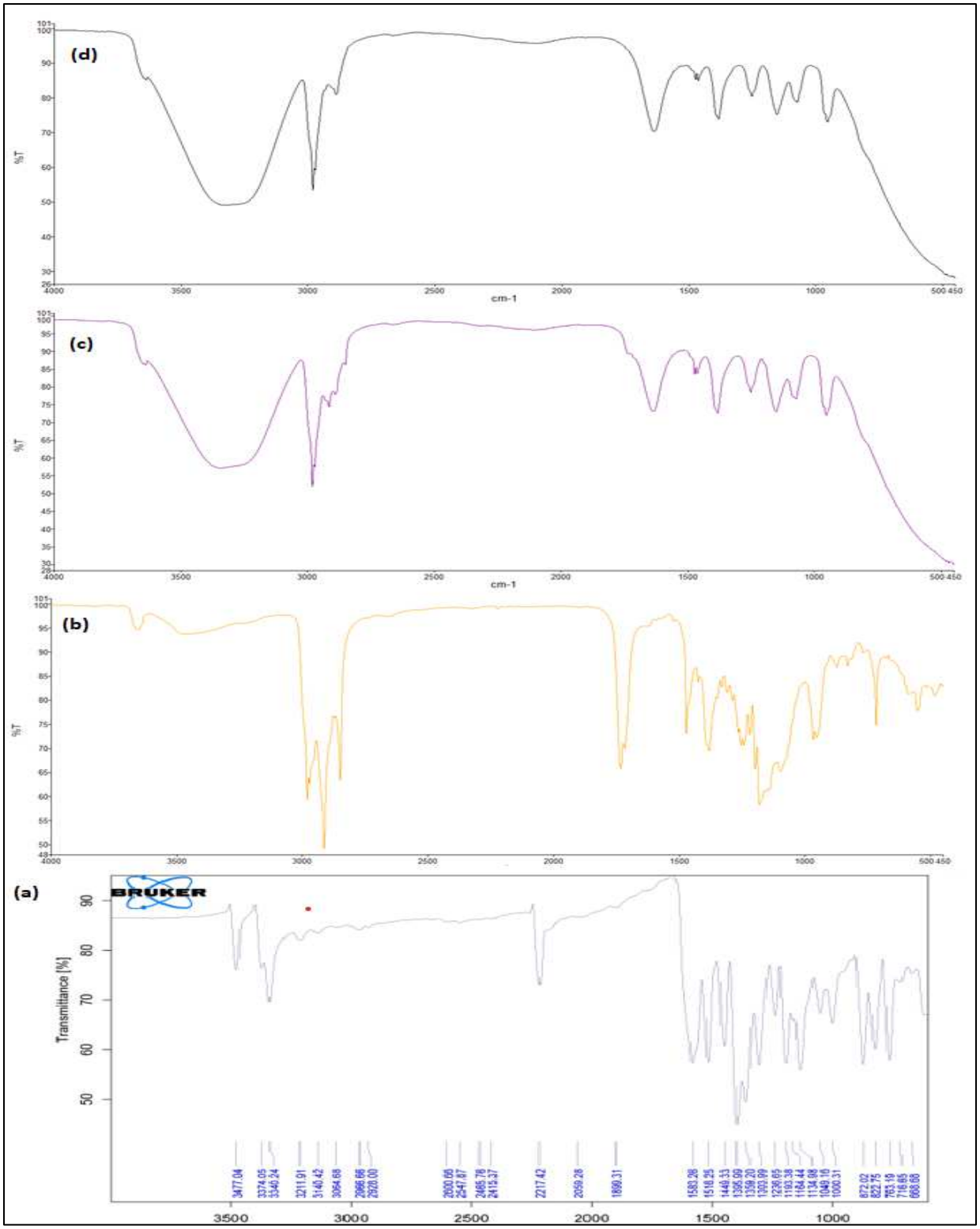

Fig 10. FTIR spectra of (a) ERVN; (b) a blend of BM + ERVN (C) LNC-Placebo (d) ERVN-TPGS-LNCs.

3.12.10. DSC thermal analysis of ERVN in an LNC system

A DSC study has typically been used to determine the alteration of melting and crystallinity behavior in the analyzed sample as a function of change in temperature via thermogram. This technique ensures the entrapment of drugs within the lipid matrix of LNCs. The present study showed that the optimized ERVN-TPGS-loaded LNCs formulation showed three peaks at 60.277 °C, 171.210 °C, and 265.201 °C, as shown in Fig 11. The 60.277 °C and 171.210 °C correlated with binary lipid and mannitol peaks [34].

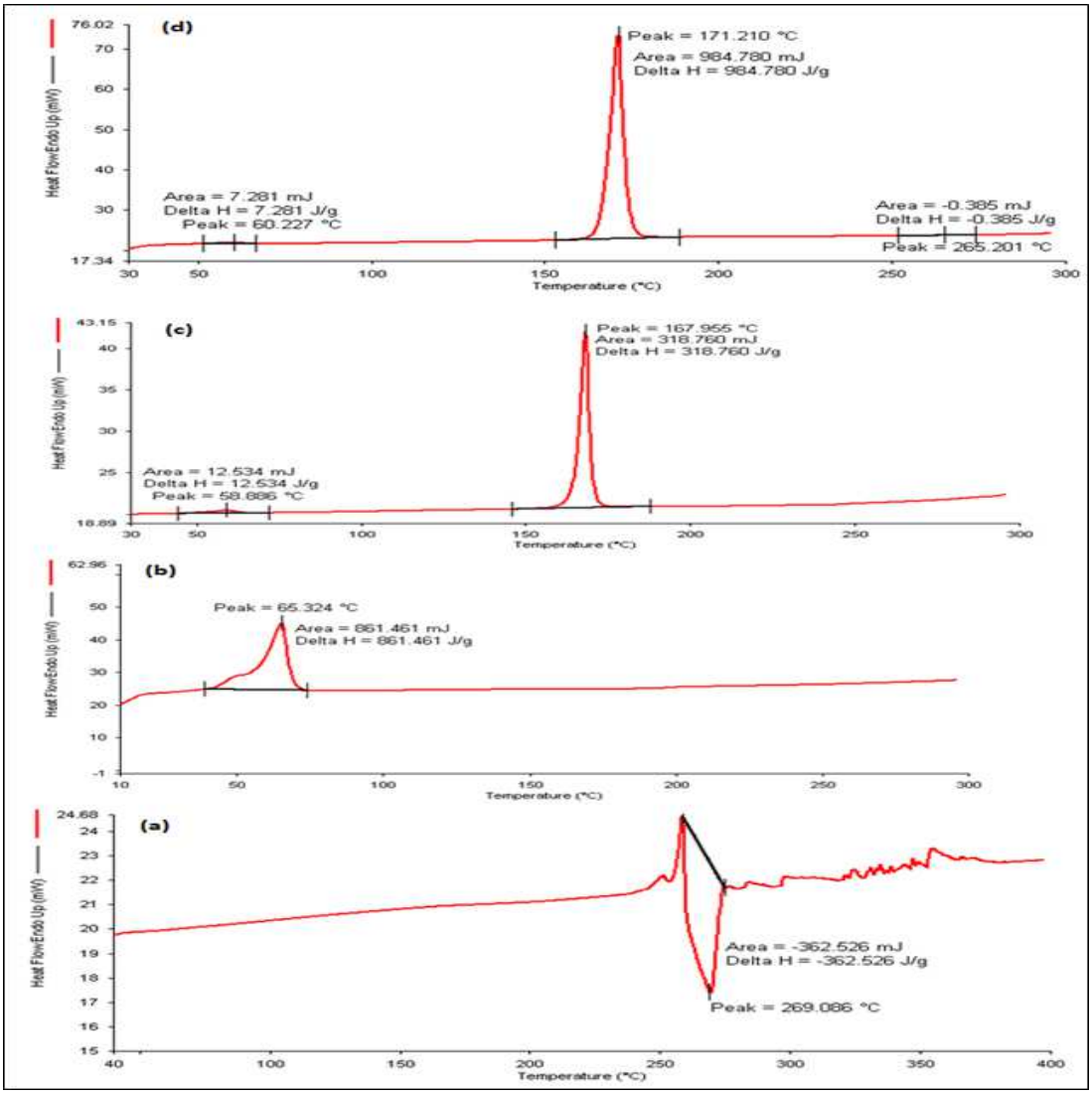

Fig 11. A DSC thermogram of (a) ERVN; (b) binary mixture; (c) LNC placebo; and (d) ERVN-TPGS-LNCs.

In addition, the peak at 265.201 °C coincided with the peak of ERVN; however, the intensity of the peak was relatively less due to the entrapment of the drug in the pores of the lipid matrix of LNCs, whereas the pure ERVN showed sharp peaks that represented the crystalline form of the drug.

3.12.11. *In-vitro* drug release

ERVN-TPGS-LNCs showed a prolonged drug release at varied pHs of 1.2, and 6.8 from an initial burst release, in contrast to ERVN-S, represented in Fig. 12, which showed a moderate drug release but not prolonged release for 24 h. The first outbreak release in LNCs was due to free ERVN adhering to the surface of the globules. Further, the drug release from an entrapped drug inside the lipid matrix of LNCs experienced surface erosion, characteristic of prolonged release nanoformulation. t50%, t75%, and dissolution profiles based on percentage cumulative drug release (%CDR) and similarity factor (f_2) were calculated for ERVN-TPGS-LNCs and EVRN-S formulation, respectively. In contrast to ERVN-S, ERVN-TPGS-LNCs showed higher % CDR at various pHs (1.2, and 6.8). Similar to % CDR, the f2-similarity factor was also estimated. The similarity values at various pH showed that the formulation, i.e., ERVN-TPGS-LNCs and the ERVN-S release pattern, were not matchable. Bellaiah and a coworker reported a similar comparison of ERVN-loaded solid lipid nanoparticle dissolution profiles or improvements in oral bioavailability [46, 47].

Table 8. A comparative dissolution profile for ERVN-TPGS-LNCs and ERVN-S in several dissolution media.

Parameters	Formulation	0.1 N HCl (pH 1.2)	PBS (pH6.8)
% CDR	ERVN-TPGS-LNCs	79.77 ± 8.35	83.23 ± 9.11
	ERVN-S	92.05 ± 8.01	94.06 ± 7.51
f2 similarity factor	_	29.65	30.43
T 50% (h)	ERVN-TPGS-LNCs	8.63	8.02

	ERVN-S	4.31	4.26
T75% (h)	ERVN-TPGS-LNCs	33.96	23.92
	ERVN-S	5.82	5.72

The kinetic drug release models were computed in the various pH buffers (1.2, and 6.8). The suitable kinetic model for drug release from LNCs was selected based on the R2 value. Therefore, the Korsmeyer Peppas kinetic release model was selected compared to other kinetic modes, including the zero-order release model, the first-order release model, the Higuchi release model, and the Korsmeyer Peppas kinetic release model, as its R2 value was close to 1 as shown in Table 8. This kinetic model explained the release patterns from the ERVN-TPGS-LNCs formulation, which are attributed to water diffusion followed by swelling and disintegration of the lipid matrix [34]. The release of drug from LNC formulations from the dialysis bag occurs by two mechanisms: (1) the release of ERVN from the lipid matrix to the donor phase without hindrance by the dialysis membrane (inside the dialysis bag); (2) the translocation of ERVN through the dialysis membrane in the receiver system (dissolution release medium). This type of drug release profile demonstrates that the drug is uniformly dispersed within the LNC matrix rather than fabricated drug enriched in the pockets or surface of the LNCs [3, 41].

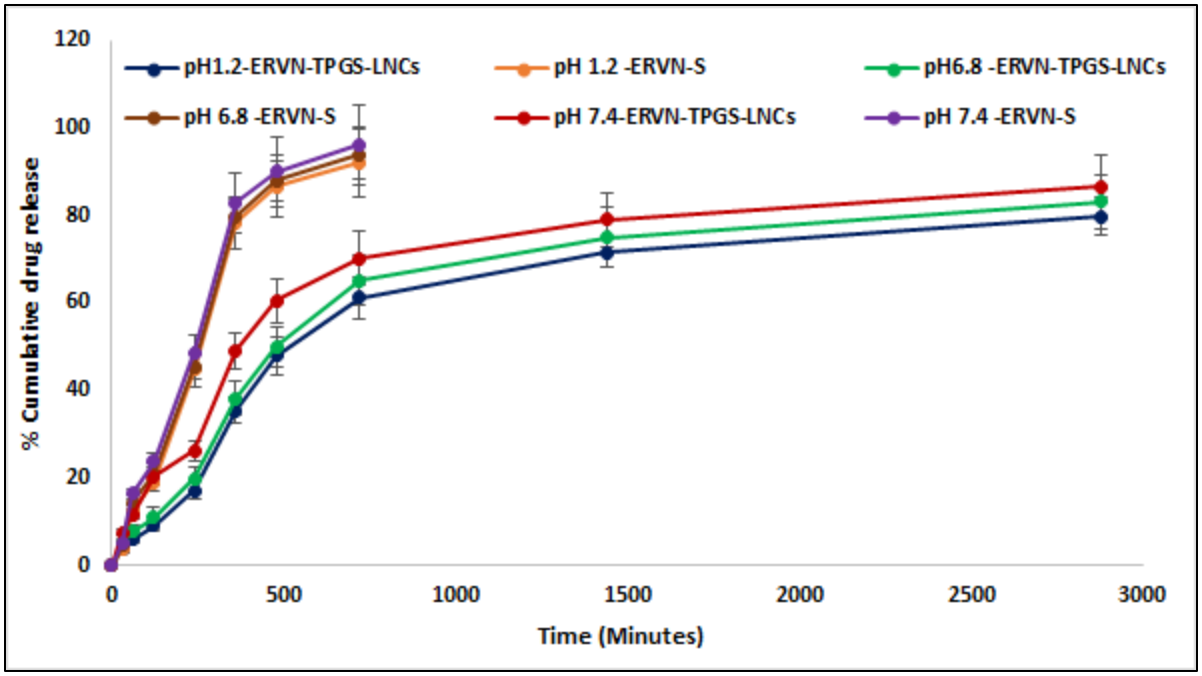

Fig 12. % CDR of ERVN from ERVN-TPGS-LNCs formulation and ERVN-S drug release in various buffers, including 0.1N HCl pH 1.2, and phosphate buffer pH 6.8.

3.12.12. *In-vitro* lipolysis

The therapeutic molecule must be solubilized close to the permeable membrane of the intestinal tract, resulting in the drugs being available for systemic circulation. So, the medicine should solubilize in the supernatant layer of the lipolysis medium (aqueous layer) and should not solubilize in the sediment layer. Fig 13 illustrates the percentage of ERVN content in each sediment and aqueous layer. The maximum solubilization of ERVN in the LNC formulation was observed in the aqueous layer, which indicated higher absorption (~74%) after administration through the oral route. Also, ERVN content in the sedimentary layer of ERVN-TPGS-LNCs was estimated and found to be 19.90 ± 82.44 %. Due to the indigestion of solid lipids in the formulation, the entrapped remained inside the lipid matrix. Hence, it has been proven that ERVN-TPGS-LNCs increased the solubilization of drugs in the aqueous medium, which mimics the gastro-intestinal

tract (GIT). As a result, it can be applied to the *in-vivo* fate of ERVN. Rehman and associates also reported a similar study in which lipophilic drug-loaded lipid-based nanocarriers showed higher drug content in the aqueous layer than in the sediment layer [48].

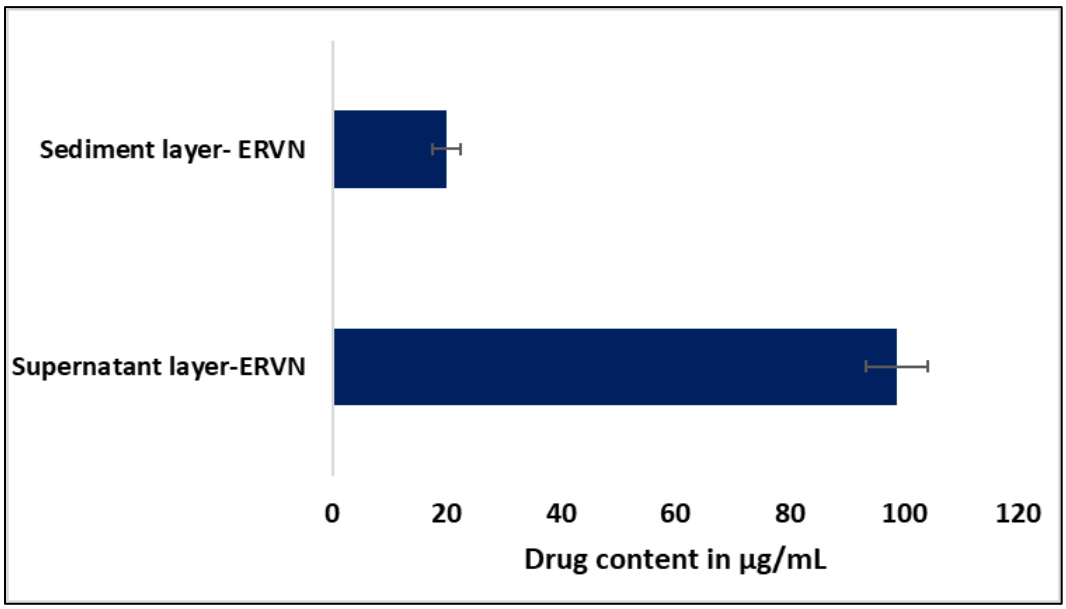

Fig. 13. Drug content (ERVN) in various layers of lipolysis media.

3.12.13. *In-vitro* Haemolysis

In haemolysis study, red blood cells (RBCs) were treated with sample or reagents, i.e., positive control (no sample or reagent was used), negative control (Triton X100 solution), ERVN-S, placebo-LNCs, and ERVN-TPGS-loaded LNCs as demonstrated in fig 14. Among the samples, the positive control revealed the least alteration in RBCs concerning their shape and structure, almost similar to the placebo-LNCs (% haemolysis was 1.73 ± 0.032%) treated with RBCs. However, in the case of negative control, the haemolysis count was very high, destabilizing the RBC membranes. Further, ERVN-S treated with RBCs showed a partial alteration in the shape of RBCs, which disarranges the membrane of RBCs (% haemolysis was 2.42 ± 0.039%). In contrast

to ERVN-S, ERVN-TPGS-loaded LNCs (% haemolysis was 1.97 ± 0.041%) were safer than pure drug suspension. Thus, it was concluded that the outcome includes the *in-vivo* fate of the drug-loaded nanoformulation. Yallapu and associates reported a similar study in which the compatibility study of herbal-loaded nanoformulations and erythrocytes was carried out to determine the toxicity of the nanoformulation in RBCs [49].

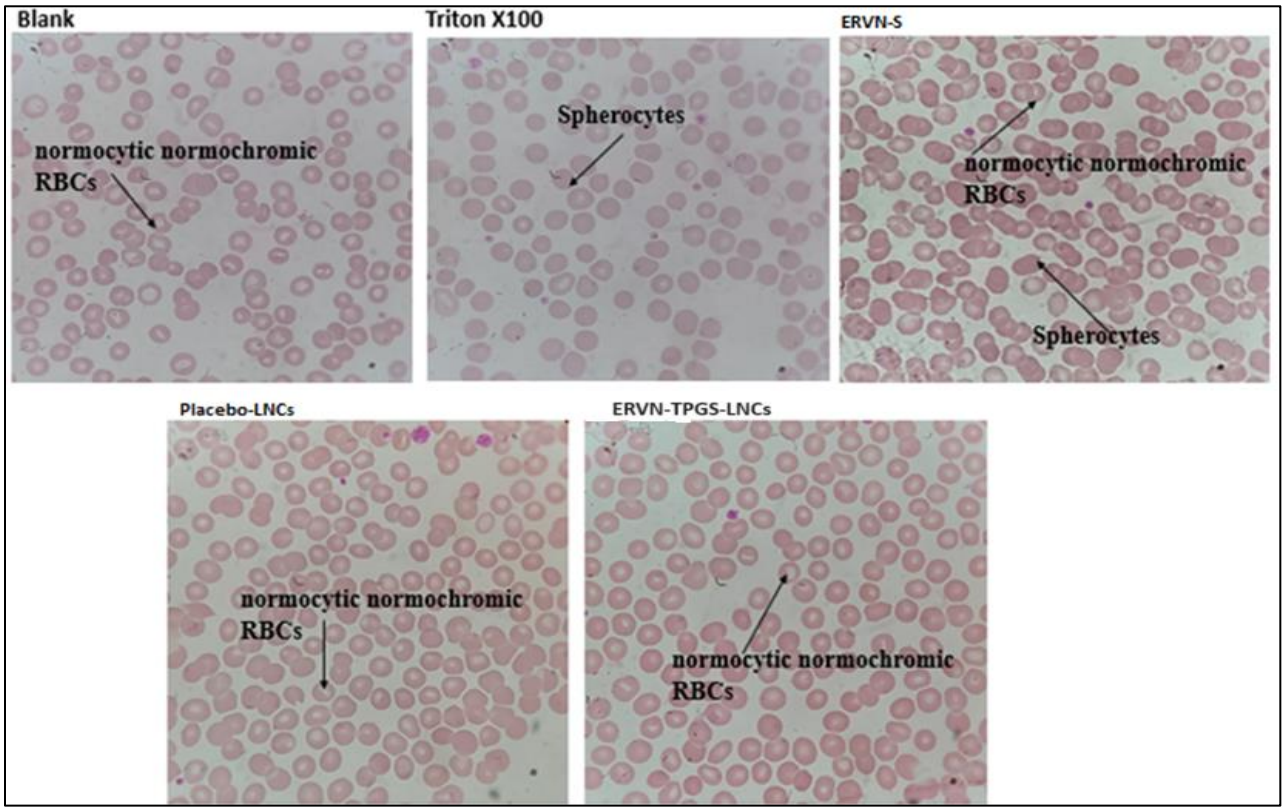

Fig 14. Figure showed haemolysis of RBCs after being treated with blank, Trition X100, ERVN-S, Placebo-LNCs, and ERVN-TPGS-LNCs.

3.12.14. Stability study in simulated gastric fluid (SGF)

The average globule size and polydispersity index of the LNCs were not substantially altered in SGF. However, significant variation ($p < 0.05$) in globule size and PDI was detected in FeSSIF and FaSSIF media. In FeSSIF, the ionic strength of the LNC formulation led to accumulation or

aggregation, which caused an alteration in globule size and PDI compared to FaSSIF, as reported in Table 9 [23].

Table 9. A stability study in gastric simulated fluid (GSF)

Time (in h)	Mean Particle Size in water (nm)	Mean Particle Size in SGF (nm)	Mean Particle Size in FaSSIF (nm)	Mean Particle Size in FeSSIF (nm)	Mean PDI in water	Mean PDI in SGF	Mean PDI in FaSSIF	Mean PDI in FeSSIF
0.5	120.82 ± 0.258	122.83 ± 0.193	124.76 ± 0.189	155.35 ± 0.218	0.173 ± 0.022	0.174 ± 0.017	0.181 ± 0.011	0.205 ± 0.016
1	121.84 ± 0.289	128.94 ± 0.201	135.34 ± 0.194	180.55 ± 0.243	0.181 ± 0.027	0.178 ± 0.019	0.188 ± 0.018	0.246 ± 0.019
2	121.74 ± 0.341	133.43 ± 0.211	143.95 ± 0.222	205.72 ± 0.304	0.181 ± 0.027	0.182 ± 0.023	0.211 ± 0.012	0.378 ± 0.014
4	122.11 ± 0.332	135.89 ± 0.213	145.88 ± 0.244	279.13 ± 0.312	0.180 ± 0.031	0.189 ± 0.024	0.211 ± 0.023	0.553 ± 0.025
6	122.43 ± 0.321	135.44 ± 0.222	149.85 ± 0.288	321.51 ± 0.323	0.182 ± 0.030	0.190 ± 0.021	0.213 ± 0.027	0.555 ± 0.028

3.12.15. Intestinal permeability study

This study estimated the flux rate through the intestinal membrane for ERVN-LNCs, ERVN-TPGS-LNCS, and their suspension. The fluxes of ERVN-LNCs and ERVN-TPGS-LNCSs were found to be 2488.285 ± 290.873 µg/cm^2/min and 2824.540 ± 320.865 µg/cm^2/min, respectively, when compared with the permeability of suspension, which was found to be 1056.491 ± 110.378 µg/cm^2/min as represented in fig 15. The apparent permeability coefficient of ERVN-S and ERVN-TPGS-LNCs were found to be 0.342 ± 0.011 x 10^{-2} and 0.916 ± 0.0873 x 10^{-2} cm/minute as shown in Table 10. The improved permeability in the LNC formulation is due to the smaller globule size, which is formed from a lipid matrix and can easily cross the intestinal membrane. ERVN-TPGS-LNCs formulation showed superior permeation and stability compared to ERVN-LNCs and ERVN-S. In addition, the presence of solutol H-15 and TPGS has a role as a p-gp efflux blocker, which assists in the improved therapeutic concentration of ERVN inside the cells, and

their flux values also confirm the permeation enhancement of ERVN by ERVN-TPGS-LNCs. Intestinal permeation may be achieved by altering the cell membrane, non-competitive and competitive inhibition of the binding region, and a resulting hindrance to ATP hydrolysis.

Further, ERVN-TPGS-LNCs have a smaller globule size, leading to improved permeability. Nabi and coworkers reported the Elvitegravir-loaded lipid-based nanocarriers (ELNCs) and performed an intestinal permeability study. The results also showed that ELNCs (small globule size) could freely cross the intestinal membrane, which showed improved permeability compared to the suspension [45].

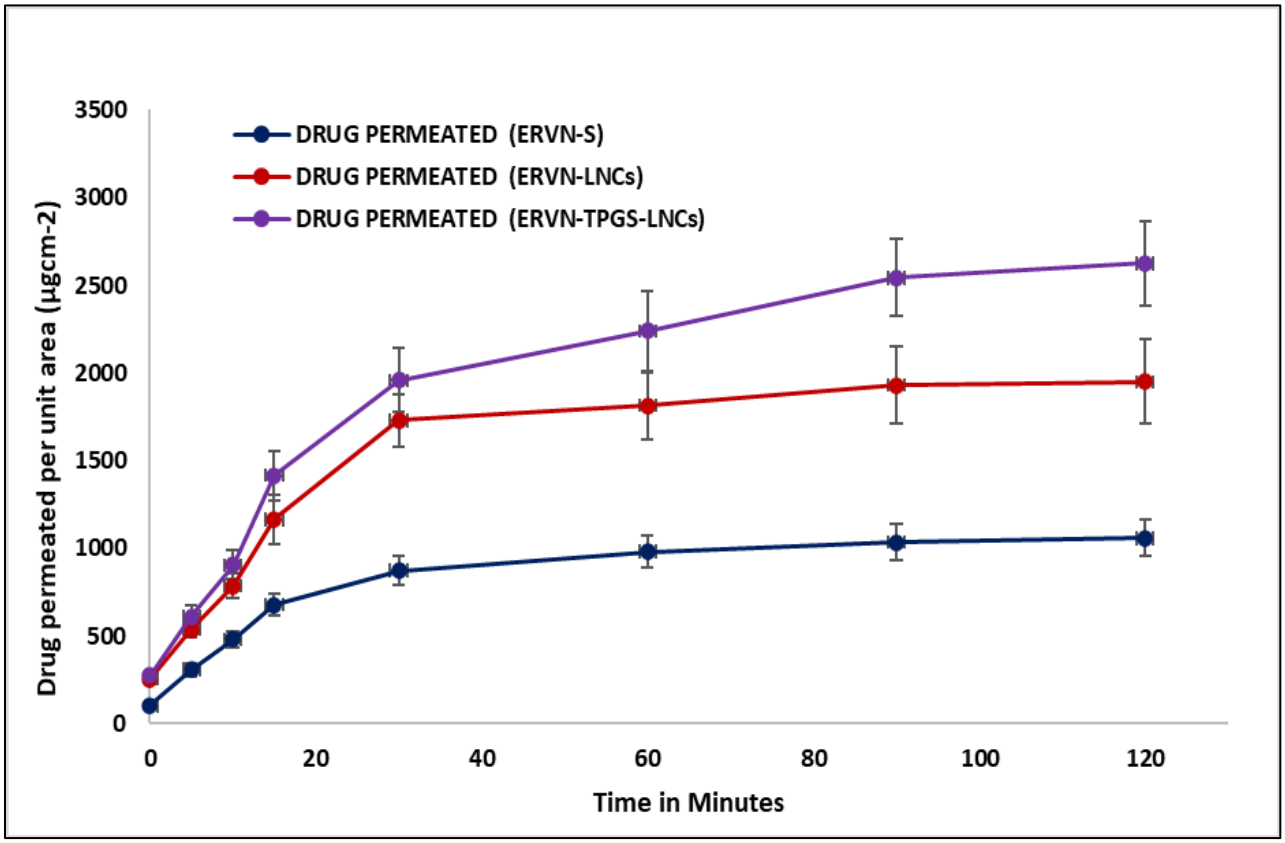

Fig 15. The drug permeated across rat intestines at different time intervals from ERVN-S, ERVN-LNCs, and ERVN-TPGS-LNCs.

Table 10. Apparent permeability coefficient of ERVN-S, ERVN-LNCs and ERVN-TPGS-LNCs.

Formulation	Papp *10-2 cm/minute
ERVN-S	0.342 ± 0.011
ERVN-LNCs	0.644 ± 0.068*
ERVN-TPGS-LNCs	0.916 ± 0.0873*

*p<0.001 compared to apparent permeability coefficient of ERVN-S.

# p<0.05 compared to apparent permeability coefficient of ERVN-S.

3.12.16. Assessment of intestinal depth permeation study using confocal laser scanning microscopy (CLSM)

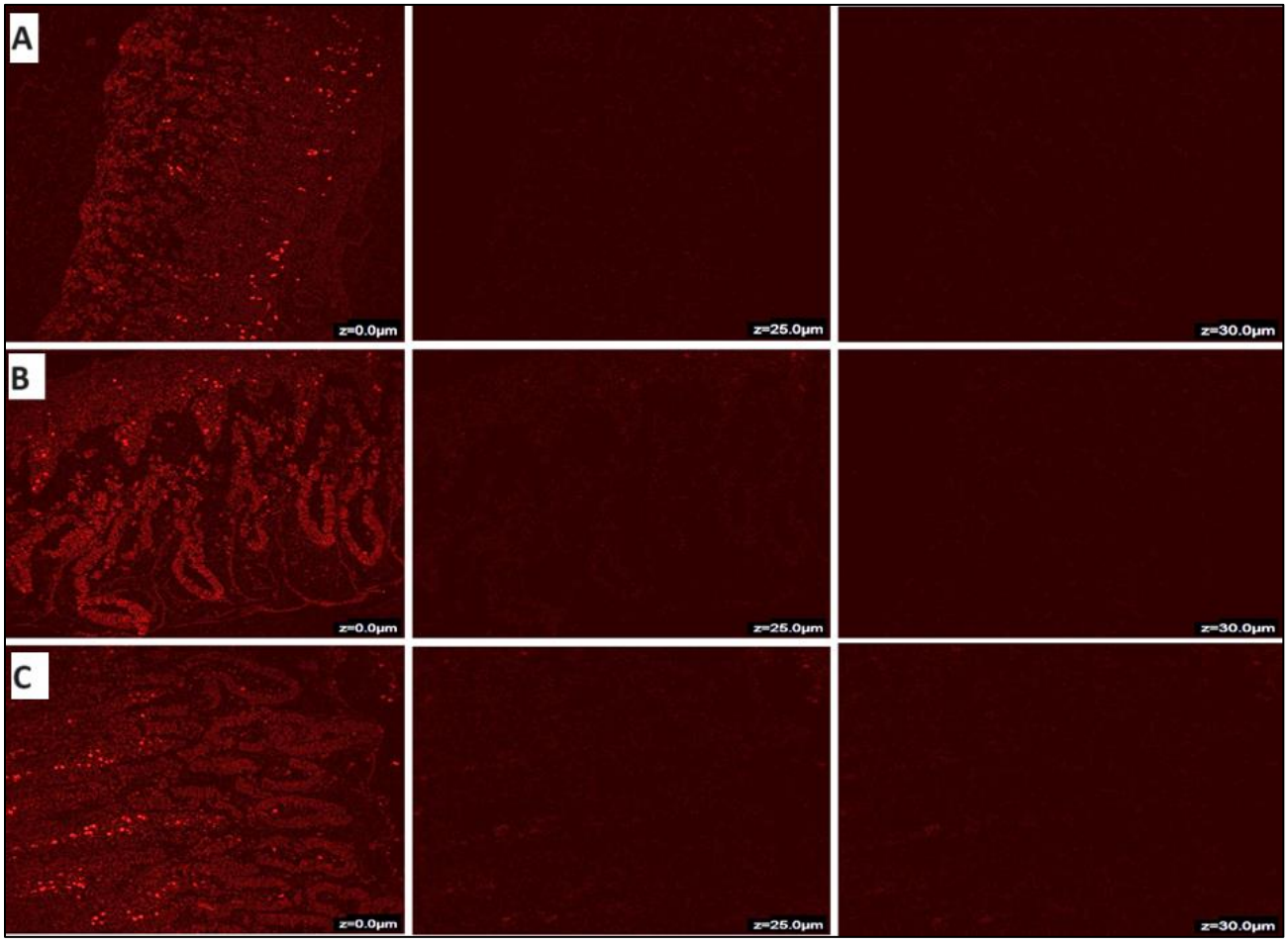

Fig. 16. Confocal images of ERVN permeation across the rat intestine- (A) ERVN-S, (B) ERVN-LNCs, and (C) ERVN=TPGS-LNCs.

CLSM was applied to assess the intestinal depth of the ERVN-loaded LNCs with or without TPGS and ERVN-S through the intestinal section. In the case of ERVN-S, the fluorescence intensity was investigated at a depth of 10µm and faded at 15 µm, as shown in Fig 16A. The maximum fluorescent intensity appeared at a depth of 15 µm in the intestinal layer while treating with ERVN-loaded LNCs, which faded at 25 µm as shown in Fig 16B. In addition, the highest fluorescence intensity of ERVN-TPGS-loaded LNCs was observed at the same depth of 15 µm as in ERVN-loaded LNCs, although it disappeared at 30 µm, as shown in Fig 16C. Increased permeation in ERVN-TPGS-loaded LNCs is due to TPGS, which acts as a potential absorption and permeation enhancer. The data showed significant permeation of ERVN across the intestinal membrane, around two-fold greater permeation than the suspension. An extensive permeation of the ERVN-TPGS-LNCs across the gut could have been due to nanoscale globules and penetration enhancers [50].

3.13. In-vivo studies

3.13.4. Pharmacokinetic study

The Pk study was carried out in wistar rats to estimate pharmacokinetic-related parameters via the oral route of administration of ERVN-TPGS-LNCs and ERVN solution, including T_{max}, C_{max}, $AUC_{0-\infty}$, AUC_{0-t}, $t_{1/2}$, and MRT as shown in fig. 17 and Table 11. The graph was plotted between drug plasma concentration versus time for calculating maximum plasma concentration (C_{max}) and time to reach peak plasma drug concentration (T_{max}). All the PK parameters were calculated using the PK solver Excel add-in tool. ERVN is a BCS class IV drug, which makes it crucial to load in an advanced drug delivery system; therefore, LNCs formulation was developed to overcome the issues related to solubility and permeability. In Table 11, C_{max} and T_{max} of ERVN-S and ERVN-TPGS-LNCSs were found to be 326.313 ng/mL and 1021.491 ng/mL; and 2 h, respectively. The

maximum plasma concentration of ERVN-TPGS-LNCs showed higher absorption because of their lipophilic property and nanosized LNCs. These properties also contribute to micellar solubilization, which enhances lymphatic uptake of ERVN via Peyer's patch of the intestine [51].

Table 11. Pharmacokinetic parameters of ERVN-S, ERVN-TPGS-LNCs, and ERVN-TPGS-LNCs + CYHD.

PK Parameters	ERVN-S	ERVN-TPGS-LNCs + CYHD	ERVN-TPGS-LNCs
Cmax (ng/mL)	326.313 ± 31.58^{*1}	845.61 ±76.72^{*1}	1021.491 ± 98.83^{*1}
Tmax (h)	2	2	2
AUC0-t (ng.h/mL)	1867.935 ± 198.58^{*1}	16700.412 ± 1875.75^{*1}	26624.648 ± 2359.37^{*1}
AUC 0−α (ng.h/mL)	15897.89 ± 1479.83^{*1}	291867.038 ± 34832.89^{*1}	553988.303 ± 60389.39^{*1}
t1/2 (h)	15.726$^{\#1}$	23.92$^{\#1}$	54.45*^{1}
MRT	8.51$^{\dagger 1}$	17.47$^{\dagger 1}$	20.807^{*1}

1 represents ERVN-S.

*, #, †, represent significant difference at $p<0.001$, $p<0.01$ and $p<0.05$, respectively.

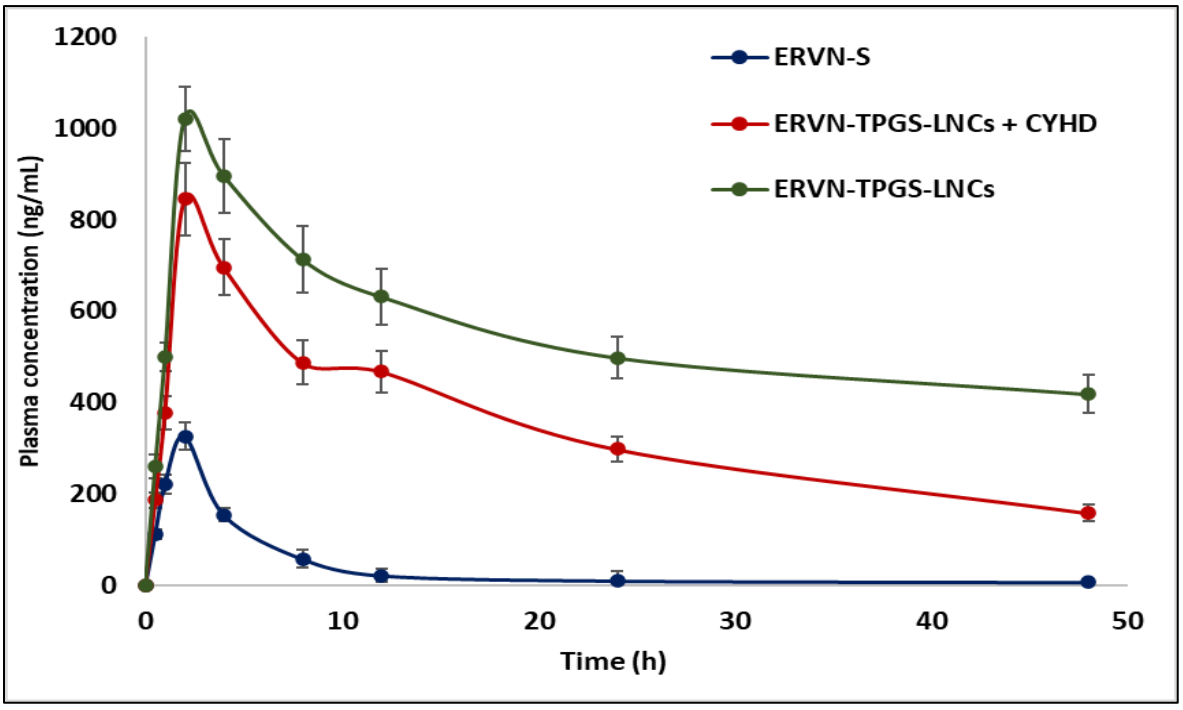

Fig 17. The plasma concentration versus time of (A) ERVN-S, ERVN-TPGS-LNCs + CYHD, and ERVN-TPGS-LNCs. Data represented in mean ± SD (n=3).

Furthermore, the Tmax value showed that the nanoformulation has prolonged drug release, correlated with in-vitro drug release. The highest absorption is attained due to the loading of lipophilic drug molecules in the ERVN-TPGS-LNCs. It was found that ERVN-TPGS-LNCs showed an ~3.13-fold increase in the bioavailability of ERVN compared to a drug suspension. The data exhibited a statistical difference between ERVN-S and ERVN-TPGS-LNCs is $p<0.001$. An increase in the area under the curve of ERVN-TPGS-LNCs was recorded compared to ERVN-S. The increased oral bioavailability of ERVN-TPGS-LNCS can also reduce the dose-related side effects of ERVN. This nanoformulation was also employed in the modulation of cytochrome P450 enzymes and p-gp efflux pumps in the intestine lumen area and increased the absorption of ERVN. The nanoformulation is generally absorbed via the lymphatic pathway in order to minimize the first-pass metabolism. It also protects the drug molecules against metabolism; hence, it assists in prolonging the drug's plasma half-life. On the other hand, enhancement in bioavailability may also be shown due to the small particle size and improved solubility of ERVN in the lipidic matrix. The globule size (less than 200 nm) might bypass gastrointestinal tract-related mucociliary clearance, leading to enhanced bioavailability and absorption of the ERVN. The improvement of the AUC of ERVN-TPGS-LNCs was recorded compared to ERVN-S. ERVN-TPGs-LNCs provided improved bioavailability to target the area of the HIV sanctuary and reduce the peripheral adverse reaction associated with the dose-related burden [52]. The data demonstrated a statistical variance of $p<0.001$ between ERVN-TPGS-LNCs and ERVN-S.

3.13.5. Chylomicron blockage model for a confirmatory test of the lymphatic uptake of ERVN-TPGS-LNCs

Earlier, the traditional surgical method was used for investigating lymphatic uptake, although the present study does not need a surgical procedure to conduct lymphatic uptake through a chylomicron blocker. The most accepted chylomicron flow blocker is a protein synthesis inhibitor

(cycloheximide). The chylomicron flow blocker prevents the generation of chylomicron, followed by blockage of M cells of phagocytic cells. Thus, it inhibits the lymphatic uptake of external molecules. In addition, no side effects or interference were observed in CYHD-treated animals. The pharmacokinetic profile of ERVN-TPGS-LNCs + CYHD (p-value) was remarkably lower than ERVN-TPGS-LNCs, which depicted the lymphatic uptake of ERVN from ERVN-TPGS-LNCs. The drug plasma concentration of ERVN-TPGS-LNCs + CYHD was low due to the prevention of chylomicron flow through the lymphatic pathway. Thus, preventing chylomicron flow leads to entry into the lymphatic pathway, which may cause the first-pass effect in the liver. In other words, the plasma drug concentration was significantly increased due to the absence of CYHD as shown in fig 17.

Additionally, TPGS and Solutol are important p-glycoprotein inhibitors and stabilizers, which also increase the secretion of chylomicrons. The nanoformulation was converted into chylomicrons after oral administration of nanoformulation, leading to lymphatic uptake; thus, it bypassed the hepatic metabolism. Herein, the ingredients of the binary mixture (Precirol ATO 5 and Labrafil 2125 CS) have a crucial role in converting the drug via lymphatic pathways by the continuous discharge of triglyceride-enriched-chylomicron. The chylomicron from the endoplasmic reticulum was released, which permits ERVN-TPGS-LNCs to enter the lymphatic pathways through enterocytes. In this transportation, LNC was sequestered through a transcellular mechanism. Increased concentration of ERVN is due to entering the chylomicron into the lymphatic pathway, which leads to bypassing the first pass metabolism in order to enhance the bioavailability of ERVN, and a similar study was performed by Garg and associates [53].

4. CONCLUSION

ERVN and TPGS (as a stabilizer and p-gp modulator) loaded LNCs were successfully fabricated and optimized by the modified solvent-based emulsion-sonication process and using CCRD-DOE, respectively. Comparative intestinal permeation showed the presence of Vit-E TPGS in the LNC formulation with improved penetration of the drugs across the intestinal membrane and increased tissue uptake. The data showed significant permeation of ERVN across the intestinal membrane with drug-encapsulated nanocarriers, around having a two-fold greater permeation than the suspension. CLSM confirmed the improvement of intestinal permeation; it was found that ERVN-TPGS-LNCs showed an approximately 2-fold higher permeation than pure suspension. Further, in a pharmacokinetic study, ERVN-TPGS-LNCs showed a 3.13-fold improvement in the bioavailability of ERVN compared to a pure drug suspension. The pharmacokinetic parameters were also aligned with intestinal permeation and CLSM. The pharmacokinetic profile of ERVN-TPGS-LNCs + CYHD (p-value) was remarkably lower than ERVN-TPGS-LNCs, which depicted the lymphatic uptake of ERVN from ERVN-TPGS-LNCs. We hypothesize that the impact of ERVN-TPGS-LNCs is to decrease the viral load with improved oral bioavailability in HIV-infected patients. ERVN-TPGS-LNCs have not been designed by any research group yet for treating HIV infection through the oral route of administration. Overall, this is a novel and effective approach that has great potential for the treatment of HIV infection.

Acknowledgements

Partially supported by the Distinguished Fellowship Program (DSFP), King Saud University, Riyadh, Saudi Arabia. The authors are also grateful to DST-PURSE for Fellowship to the first author. The authors are also grateful to DST-FIST for facilities at Jamia Hamdard, IIT-Delhi,

SAIF- AIIMS, and Central Instrument Facility in Jamia Millia Islamia for providing research facilities.

Author contributions

Abdul Muheem: Conceptualization, Preparation, Characterization, Analysis, Writing Original Draft.

Mohd Waseem: Assisted in animal handling and pharmacokinetic studies.

Eman Aldosari: Writing and Reviewing.

Sanjula Baboota: Co-supervisor, Reviewing, Editing, and Visualization.

Javed Ali: Supervisor, Data Validation, Reviewing, Editing, and Project execution. Corresponding author.

Funding: The financial support to the corresponding author from King Saud University under the Distinguished Fellowship Program is acknowledged. We acknowledge financial support from the DST-PURSE for Fellowship to the first author. The authors also thank DST-FIST for financial support at Jamia Hamdard, New Delhi.

Institutional review board statement: "*The animal study protocol was permitted by the Institutional Animal Ethical Committee (IAEC) (Jamia Hamdard, New Delhi, India), with the approved animal study protocol 173/CPCSEA, 28th Jan 2000 (Approval No. 1706, 2021).”*

Data availability:

The dataset used or analysed during the current research work will be provided from the corresponding author on reasonable request.

Declarations

Conflict of interest: The authors declare that there is no conflict of interest. The funding body had no role in the designing of the research work, in performing experiments, analyzing the data, drafting the manuscript, or in the decision to publish the dataset.

List of Abbreviations

LNCs	Lipid based nanocarriers
TPGS	d-alpha-tocopheryl polyethylene glycol 1000 succinate
ERVN	Etravirine,
HIV	Human immunodeficiency virus
AIDS	Acquired immunodeficiency syndrome
ARD	Anti-retroviral drug
TEM	Transmission electron microscopy
PDI	Polydispersity index
STDs	Sexually transmitted diseases
cDNA	Complementary DNA
HAART	Highly active anti-retroviral therapy
NNRTI	Nucleoside reverse transcriptase inhibitor
BCS	Biopharmaceutical classification system
Rt	Retention time
SLs	Solid lipids
CI	Crystallinity index
BM	Binary mixture
QTPP	Quality target product profile
QbD	Quality by design
CPP	Critical process parameters
CCRD	Central composite rotatable design
CQA	Critical quality attributes

SLS	Sodium lauryl sulfate
CDR	Cumulative drug release
OD	Optical density
EE	Entrapment efficiency
RSM	Response surface methodology
FTIR	Fourier transform infrared spectroscopy
DSC	Differential Scanning Calorimetry
SGF	Simulated gastric fluid
PBS	Phosphate buffer saline
FeSSIF	Fed state simulated intestinal fluid
FaSSIF	Fasted state simulated intestinal fluid
ANOVA	Analysis of variance

References

1. Baba TW, Liska V, Hofmann-Lehmann R, Vlasak J, Xu W, Ayehunie S, Cavacini LA, Posner MR, Katinger H, Stiegler G, Bernacky BJ, Rizvi TA, Schmidt R, Hill LR, Keeling ME, Lu Y, Wright JE, Chou TC, Ruprecht RM. Human neutralizing monoclonal antibodies of the IgG1 subtype protect against mucosal simian-human immunodeficiency virus infection. Nat Med. 2000; 6(2): 200-6.

2. UNAIDS Global AIDS Update 2023. https://www.unaids.org/en/resources/documents/2023/in-danger-global-aids-update (Assessed on 20 August 2023).

3. Rojekar S, Abadi LF, Pai R, Mahajan K, Kulkarni S, Vavia PR. Multi-organ targeting of HIV-1 viral reservoirs with Etravirine loaded nanostructured lipid carrier: An in-vivo proof of concept. Eur J Pharm Sci. 2021; 164: 105916.

4. Blankson JN, Persaud D, Siliciano RF. The challenge of viral reservoirs in HIV-1 infection. Annu. Rev. Med. 2002; 53: 557–593.

5. Kuo HH, Lichterfeld M. Recent progress in understanding HIV reservoirs. Curr. Opin. HIV AIDS. 2018; 13: 137–142.

6. Liu Y Chen, C. Role of nanotechnology in HIV/AIDS vaccine development. Adv Drug Deliv Rev. 2016; 103: 76–89.

7. Agrawal N, Rowe J, Lan J, Yu Q, Hrycyna CA, Chmielewski J. Potential tools for eradicating HIV reservoirs in the brain: development of trojan horse prodrugs for the inhibition of P-glycoprotein with anti-HIV-1 activity. J Med Chem. 2020; 63(5): 2131–8.

8. Puligujja P, McMillan JE, Kendrick L, Li T, Balkundi S, Smith N, Veerubhotla RS, Edagwa BJ, Kabanov AV, Bronich T, Gendelman HE, Liu XM. Macrophage folate receptor-targeted anti-retroviral therapy facilitates drug entry, retention, anti-retroviral activities and biodistribution for reduction of human immunodeficiency virus infections. Nanomed. Nanotechnol., Biol. Med. 2013; 9: 1263–1273.

9. Amin ML. P-glycoprotein Inhibition for Optimal Drug Delivery. Drug Target Insights. 2013; 7: 27-34.

10. Kakuda TN, Smedt GD, Leemans R, Peeters M, Vyncke V, Solingen-ristea RV, Woodfall B, Hoetelmans R. Bioavailability of Etravirine 200mg administered as a single 200-mg tablet versus two 100-mg tablets in HIV-negative, healthy volunteers. Adis Insight. 2011: 20605.

11. Johnson LB, Saravolatz LD. Etravirine, a next-generation nonnucleoside reverse-transcriptase inhbitor. Clin. Infect. Dis. 2009; 48: 1123–1128.

12. Jindal AB, Bachhav SS, Devarajan PV. In situ hybrid nano drug delivery system (IHN-DDS) of anti-retroviral drug for simultaneous targeting to multiple viral reservoirs: an in vivo proof of concept. Int. J. Pharm. 2017; 521: 196–203.

13. Dash PK, Gendelman HE, Roy U, Balkundi S, Alnouti Y, Mosley RL, Gelbard HA, McMillan J, Gorantla S, Poluektova LY. Long-acting nanoformulated anti-retroviral therapy elicits potent anti-retroviral and neuroprotective responses in HIV-1-infected humanized mice. AIDS. 2012; 26: 2135–2144.

14. Li W, Wu J, Zhan P, Chang Y, Pannecouque C, De Clercq E, Liu X. Synthesis, drug release and anti-HIV activity of a series of PEGylated zidovudine conjugates. Int. J. Biol. Macromol. 2012; 50: 974–980.

15. Taneja S, Shilpi S, Khatri K. Formulation and optimization of efavirenz nanosuspensions using the precipitation-ultrasonication technique for solubility enhancement. Artif. Cells, Nanomed. Biotechnol. 2016; 44: 978–984.

16. Economidou SN, Lamprou DA, Douroumis D. 3D printing applications for transdermal drug delivery. Int. J. Pharm. 2018; 544: 415–424.

17. Nowacek AS, Miller RL, McMillan JE, Kanmogne G, Kanmogne M, Mosley RL, Ma Z, Graham S, Chaubal M, Werling J, Rabinow B, Dou H, Gendelman HE. NanoART synthesis, characterization, uptake, release and toxicology for human monocyte-macrophage drug delivery. Nanomed. 2009; 4: 903–917.

18. Misra A, Kher G. Drug delivery systems from nose to brain. Curr. Pharm. Biotechnol. 2012; 13: 2355–2379.

19. Khan S, Shaharyar M, Fazil M, Hassan MQ, Baboota S, Ali J. Tacrolimus loaded nanostructured lipid carriers for oral delivery-in vivo bioavailability enhancement. Eur. J. Pharm. Biopharm. 2016; 109: 149–157.

20. Agrawal M, Saraf S, Saraf S, Dubey SK, Puri A, Patel RJ, Ajazuddin, Ravichandiran V, Murty US, Alexander A. Recent strategies and advances in the fabrication of nano lipid carriers and their application towards brain targeting. J. Control. Rel. 2020; 321: 372–415.

21. Negi LM, Jaggi M, Talegaonkar S. Development of protocol for screening the formulation components and the assessment of common quality problems of nanostructured lipid carriers. Int. J. Pharm. 2014; 461 (1-2): 403–4.

22. Qamar Z, Ashhar MU, Annu, Qizilibash FF, Sahoo PK, Ali A, Ali J, Baboota S. Lipid nanocarrier of selegiline augmented anti-Parkinson's effect via P-gp modulation using quercetin. Int. J of Pharm. 2021; 609: 121131.

23. Alam T, Khan S, Gaba B, Haider MF, Baboota S, Ali J. Adaptation of Quality by Design-Based Development of Isradipine Nanostructured-Lipid Carrier and Its Evaluation for In Vitro Gut Permeation and In Vivo Solubilization Fate. J. Pharm. Sci. 2018; 107: 2914–2926.

24. Neupane YR, Srivastava M, Ahmad N, Kumar N, Bhatnagar A, Kohli K. Lipid based nanocarrier system for the potential oral delivery of decitabine: Formulation design, characterization, ex vivo, and in vivo assessment. Int. J. Pharm. 2014; 477 (1-2): 601–612.

25. Luiz MT, Filippo LDD, Alves RC, Araújo VHS, Duarte JL, Marchetti JM, Chorilli M. The use of TPGS in drug delivery systems to overcome biological barriers. Europ Polymer J, 2021; 142: 110129.

26. Gurumukhi VC, Bari SB. Quality by design (QbD)-based fabrication of atazanavir-loaded nanostructured lipid carriers for lymph targeting: bioavailability enhancement using chylomicron flow block model and toxicity studies. Drug Delivery and Translational Research. 2022; 12(5): 1230-1252.

27. Jain A, Hurkat P, Jain, SK. Development of liposomes using formulation by design: Basics to recent advances. Chemis and Phys of Lipids. 2019; 224: 104764.

28. Iqubal MK, Kamal A, Iqubal A, Imran M, Ali J, Baboota S. Development and validation of a robust HPLC method for simultaneous estimation of 5-fluorouracil and resveratrol and its application in the engineered nanostructured lipid carrier, Curr. Anal. Chem. 2021; 17: 385–395.

29. Blanco KC, De Lima CJB, Monti R, Martins J, Bernardi NS, Contiero J. Bacillus lehensis - An alkali-tolerant bacterium isolated from cassava starch wastewater: Optimization of parameters for cyclodextrin glycosyltransferase production. Ann. Microbiol. 2012; 62: 329–337.

30. Singh A, Neupane YR, Mangla B, Kohli K. Nanostructured Lipid Carriers for Oral Bioavailability Enhancement of Exemestane: Formulation Design, In Vitro, Ex Vivo, and In Vivo Studies. J. Pharm. Sci. 2019; 108: 3382–3395.

31. Mishra N, Sharma S, Deshmukh R, Kumar A, Sharma R. Development and Characterization of Nasal Delivery of Selegiline Hydrochloride Loaded Nanolipid Carriers for the Management of Parkinson's Disease. Cent. Nerv. Syst. Agents Med. Chem. 2019; 19 (1): 46–56.

32. González-Mira E, Nikolić S, García ML, Egea MA. Souto EB, Calpena AC. "Potential use of nanostructured lipid carriers for topical delivery of flurbiprofen," J of Pharma Sci, 2011; 100(1): 242–251.

33. Joshi AS, Patel HS, Belgamwar VS, Agrawal A, Tekade AR. "Solid lipid nanoparticles of ondansetron HCl for intranasal delivery: development, optimization and evaluation," Journal of Materials Science: Materials in Medicine, 2012; 23(9): 2163–2175.

34. Sartaj A, Alam M, Biswas L, Shahar Yar M, Mir SR, Verma AK, Baboota S, Ali J. Combinatorial delivery of Ribociclib and green tea extract mediated nanostructured lipid carrier

for oral delivery for the treatment of breast cancer synchronising in silico, in vitro, and in vivo studies. J Drug Target. 2022; 30(10): 1113-1134.

35. Innes A, Farrell AM, Burden RP, Morgan AG, Powell RJ. Complement activation by cellulosic dialysis membranes. J Clin Pathol. 1994; 47(2):155-158.

36. Salome AC, Godswill CO, Ikechukwu IO. Kinetics and mechanisms of drug release from swellable and non swellable matrices: a review. Res J Pharm Biol Chem Sci. 2013.

37. Cruz Silva MM, Madeira VMC, Almeida LM, Custódio JBA. Hemolysis of human erythrocytes induced by tamoxifen is related to disruption of membrane structure. Biochim Biophys Acta – Biomembr. 2000; 1464(1): 49–61.

38. Khan S, Ganguli M, Aditya A, Khan S, Baboota S, Ali J. Improved in vivo performance and immunomodulatory effect of novel Omega-3 fatty acid-based Tacrolimus nanostructured lipid carrier. J. Drug. Deliv. Sci. Technol. 2019; 52: 138-149.

39. Attari Z, Bhandari A, Jagadish PC, Lewis S. Enhanced ex vivo intestinal absorption of olmesartan medoxomil nanosuspension: Preparation by combinative technology. Saudi Pharm J. 2016; 24(1): 57-63.

40. Lee J, Kang S, Park H, Sun JG, Kim EC, Shim G. Nanoparticles for Lymph Node-Directed Delivery. Pharmaceutics. 2023; 15(2): 565.

41. Pai RV, Vavia PR. Chitosan oligosaccharide enhances binding of nanostructured lipid carriers to ocular mucins: effect on ocular disposition. Int. J. Pharm. 2020; 577: 119095.

42. Tarsitano M, Cristiano MC, Mancuso A, Barone A, Torella D, Paolino D. Lipid-Based Formulations Containing Labrafil M2125-CS: A Deep Investigation on Nanosystem Stability, Nanomanufact. 2022; 2(1): 41-52.

43. Malamatari M, Taylor KM, Malamataris S, Douroumis D, Kachrimanis K. Pharmaceutical nanocrystals: production by wet milling and applications, Drug Discov. Today. 2018; 23(3): 534–547.

44. Emami J, Yousefian H, Sadeghi H. Targeted nanostructured lipid carrier for brain delivery of artemisinin: Design, preparation, characterization, optimization and cell toxicity. J. Pharm. Pharm. Sci. 2018; 21: 225s–241s.

45. Nabi B, Rehman S, Aggarwal S, Baboota S, Ali J. Quality by Design Adapted Chemically Engineered Lipid Architectonics for HIV Therapeutics and Intervention: Contriving of Formulation, Appraising the In vitro Parameters and In vivo Solubilization Potential. AAPS PharmSciTech. 2020; 21(7): 261.

46. Annu, Baboota S, Ali J. In vitro appraisals and ex vivo permeation prospect of chitosan nanoparticles designed for schizophrenia to intensify nasal delivery. Polym Bull. 2022; 79(4): 2263–2223.

47. Bellaiah PG, Hagalavadi NS, Madalli RK. 23 Factorial Design: An Approach For Formulation of Solid Lipid Nanoparticles of Etravirine for Oral Administration. Ind J of Pharma Sci, 2022: 1-11.

48. Rehman S, Nabi B, Baboota S, Ali J. Tailoring lipid nanoconstructs for the oral delivery of paliperidone: Formulation, optimization and in vitro evaluation, Chem and Phys of Lipids, 2021; 234: 105005.

49. Yallapu MM, Ebeling MC, Chauhan N, Jaggi M, Chauhan SC. Interaction of curcumin nanoformulations with human plasma proteins and erythrocytes. Int J Nanomed. 2011; 6: 2779-90.

50. Khan SA, Rehman S, Nabi B, Iqubal A, Nehal N, Fahmy UA, Kotta S, Baboota S, Md S, Ali J. Boosting the brain delivery of Atazanavir through nanostructured lipid carrier-based approach for mitigating neuroaids. Pharmaceutics, 2020; 12: 1–26.

51. Muheem A, Baboota S, Ali J. An in-depth analysis of novel combinatorial drug therapy via nanocarriers against HIV/AIDS infection and their clinical perspectives: a systematic review, Expert Opin Drug Deliv. 2021; 18(8): 1025-1046.

52. Inugala S, Eedara BB, Sunkavalli S, Dhurke R, Kandadi P, Jukanti R, Bandari S. Solid self-nanoemulsifying drug delivery system (S-SNEDDS) of darunavir for improved dissolution and oral bioavailability: In vitro and in vivo evaluation. Euro J of Pharma Sci, 2015; 74: 1-10.

53. Garg B, Beg S, Kaur R, Kumar R, Katare OP, Singh B. Long-chain triglycerides-based self-nanoemulsifying oily formulations (SNEOFs) of darunavir with improved lymphatic targeting potential. J of Drug Target, 2018; 26(3): 252-266.